Zhou, Z., Liu, A., Xia, S., Leung, C., Qi, J., Meng, Y., Xie, W., Park, P., Collingridge, G. L., & Jia, Z. (2018). The C-terminal tails of endogenous GluA1 and GluA2 differentially contribute to hippocampal synaptic plasticity and learning. *Nature Neuroscience*, *21*(1), 50-62. https://doi.org/10.1038/s41593-017-0030-z

Title: The C-Terminal tails of endogenous GluA1 and GluA2 differentially contribute to hippocampal synaptic plasticity and learning

Authors: Zikai Zhou[1,2,3,6], An Liu[3,6], Shuting Xia[1,2,3,6], Celeste Leung[1,2,6], Junxia Qi[3], Yanghong Meng[1,2], Wei Xie[3], Pojeong Park[2,4,5], Graham L. Collingridge[2,4,5], and Zhengping Jia[1,2]

Affiliations: [1]Neurosciences & Mental Health, The Hospital for Sick Children, 555 University Ave., Toronto, Ontario, Canada M5G 1X8

[2]Department of Physiology, Faculty of Medicine, University of Toronto, 1 King's College Circle, Toronto, Ontario, Canada M5S 1A8

[3]The Key Laboratory of Developmental Genes and Human Disease, Ministry of Education, Institute of Life Sciences, Southeast University, Nanjing, China; Co-innovation Center of Neuroregeneration, Nantong University, Nantong, China

[4]Lunenfeld-Tanenbaum Research Institute, Mount Sinai Hospital, 600 University Avenue Toronto, Ontario, Canada M5G 1X5

[5]Centre for Synaptic Plasticity, Department of Physiology, Pharmacology & Neuroscience, Dorothy Hodgkin Building, University of Bristol, Bristol, BS1 3NY, UK

[6]These authors contributed equally to the paper

Correspondence should be addressed to Zhengping Jia at zhengping.jia@sickkids.ca and Graham Collingridge at collingridge@lunenfeld.ca. All requests for materials should be directed to Zhengping Jia at zhengping.jia@sickkids.ca

Short Title: GluA1 and GluA2 Specify Bidirectional Plasticity

Summary

Long-term potentiation (LTP) and depression (LTD) at glutamatergic synapses are intensely investigated processes for understanding the synaptic basis for learning and memory, but the underling molecular mechanisms remain poorly understood. We have made three novel mouse lines where the C-terminal domains (CTDs) of endogenous AMPA receptors (AMPARs), the principal mediators of fast excitatory synaptic transmission, are specifically exchanged. These mice display profound deficits in synaptic plasticity without any effects on basal synaptic transmission. Our study reveals that the CTDs of GluA1 and GluA2, the key subunits of AMPARs, are necessary and sufficient to drive NMDA receptor-dependent LTP and LTD, respectively. In addition, these domains exert differential effects on spatial and contextual learning and memory. These results establish dominant roles of AMPARs in governing bidirectional synaptic and behavioral plasticity in the CNS.

Long-term potentiation (LTP) and depression (LTD) are the most extensively studied forms of synaptic plasticity, widely regarded as the cellular basis for learning and memory[1-3]. Deficits in LTP and LTD are associated with animal models of many neurological and mental disorders[4]. Thus, the mechanisms governing these forms of plasticity have been the subject of intensive investigations during the last few decades. Numerous studies have focused on the AMPA subtype of glutamate receptors (AMPARs) because these receptors are the principal mediator of fast, excitatory synaptic transmissions in the mammalian CNS. This has led to a major hypothesis that GluA1 and GluA2, the key subunits of AMPARs, are crucial for LTP and LTD, respectively[5-8]. However, this idea has been challenged in recent genetic studies showing that both LTP and LTD can be established in the absence of AMPAR

subunits[8-11]. Therefore, despite intense studies, the fundamental mechanisms underlying synaptic plasticity remain elusive[4,8].

A major reason for the controversy is that many previous studies have employed exogenously expressed, non-physiological homomeric receptors (e.g. refs 12,13), whose behavior may not be the same as the more commonly expressed native, hetero-tetrameric AMPARs. Small peptides have been used to disrupt protein interactions at endogenous AMPARs[13-18], but they have the limitation of potential off-target effects. Genetic studies (e.g. global or conditional KO mice) have also been compromised by the formation of non-physiological receptors, leading to dramatic alterations in baseline AMPAR properties or synaptic function[9,10,19-21], which makes the interpretation inconclusive. Specifically, the ablation of the GluA1 subunit causes impairments in receptor assembly and trafficking[9,22] and consequently a drastic reduction in basal synaptic transmission[9,10,20,23], which confounds the analysis of synaptic plasticity. Similarly, deletion of the GluA2 subunit results in the formation of aberrant receptors[24], altered biophysical properties and severely reduced synaptic strength[9,11,19,21]. Significantly, GluA2-lacking receptors are Ca^{2+} permeable and their activation can induce various forms of plasticity[19,25] that can alter the physiology of neurons and, in some cases, even trigger cell death[26]. In studies using mice where all major AMPAR subunits are deleted using a cell-specific Cre/loxP method[9-11], synaptic mechanisms in these mice will unlikely reflect those operating under normal physiological conditions, where the full native AMPAR complement is present. Knock in (KI) mouse models involving mutations of individual amino acids of AMPARs have been created but are limited by relatively mild phenotypes and therefore have not been able to provide definitive answers[27,28].

Therefore, we reasoned that removing the entire subunit of GluA1 or GluA2 is not an ideal approach to address the role of AMPARs in plasticity. We therefore have developed three new mouse models where only specific domains of endogenous AMPARs are switched, which allowed synaptic plasticity to be systematically and definitively analyzed without confounding effects on basal synaptic transmission. Using these mice we revealed that the CTDs of native GluA1 and GluA2 are necessary and sufficient for LTP and LTD expression, respectively and regulate distinct forms of learning and memory.

RESULTS

Basal synaptic and AMPAR properties in GluA1^{C2KI} and GluA2^{C1KI} mice

We used the homologous recombination strategy in ES cells to generate three novel CTD replacement mutant mice: GluA1^{C2KI} where the CTD of GluA1 was replaced by that of GluA2, GluA2^{C1KI} where the CTD of GluA2 was replaced by that of GluA1, and, by crossing these two strains, GluA1^{C2KI}/GluA2^{C1KI} where the CTDs of GluA1 and GluA2 were swapped (**Fig. 1a**,**b** and **Supplementary Fig. S1**, **S2**). The CTD replacements in these mice were confirmed by PCR and Southern blot analysis of ES cell and tail DNA followed by western blot analysis of the brain protein lysates (**Supplementary Fig. S1, Fig. S2a-e, Fig. S9 and Fig. S10**). In contrast to GluA2 KO mice, which exhibited increased mortality, growth retardation and severe motor deficits[19,29], neither GluA1^{C2KI} nor GluA2^{C1KI} mice showed any alterations in viability, developmental growth, life span, fertility or home-cage behaviors. Histochemical analyses showed that both strains of mice have intact brain structure, normal synapse (**Supplementary Fig. S2f,g**) and AMPAR distribution profiles (**Supplementary Fig. S2h,i**) in the hippocampus.

To examine basal synaptic and AMPAR properties in these mice, we first compared input/output curves of field excitatory postsynaptic potentials (fEPSPs), but found no significant differences between WT,

GluA1^{C2KI} (**Fig. 1c**) and GluA2^{C1KI} (**Fig. 1d**) mice. Next, we used whole-cell patch-clamp recordings of CA1 neurons to examine excitatory postsynaptic currents (EPSCs) mediated by NMDARs ($EPSC_{NMDAR}$) and AMPARs ($EPSC_{AMPAR}$), but found no differences in $EPSC_{NMDAR}/EPSC_{AMPAR}$ ratios between WT, GluA1^{C2KI} and GluA2^{C1KI} mice (**Fig. 1e**). This was in marked contrast to GluA2 KO mice that showed a 3-fold increase in the $EPSC_{NMDAR}/EPSC_{AMPAR}$ ratio, indicative of the severe reduction in AMPAR-mediated EPSCs in these mice[15,25,26] (**Fig. 1e**). Consistent with the lack of effect on basal synaptic transmission, we found no differences in the frequency or amplitude of miniature EPSCs (mEPSCs) between WT, GluA1^{C2KI} and GluA2^{C1KI} mice (**Fig. 1f**). Since the deletion of GluA1 causes a dramatic reduction in surface extra-synaptic AMPARs[9,10,23], we assessed glutamate evoked currents in outside-out patch experiments, but found no significant differences between WT, GluA1^{C2KI} and GluA2^{C1KI} mice (**Fig. 1g**). To assess the ion channel properties of AMPARs, we analyzed the current/voltage (I/V) relationship of AMPAR-mediated currents, but again found no differences between WT, GluA1^{C2KI} and GluA2^{C1KI} mice (**Fig. 1h**). The linear I/V curves in these mice differ clearly from the strongly rectified I/V relationship of GluA2 KO mice (**Fig. 1h**,**i**), indicating that channel properties (including polyamine sensitivity, receptor composition and Ca^{2+} permeability) of AMPARs are not altered in GluA1^{C2KI} or GluA2^{C1KI} mice. Furthermore, NMDAR channel properties as indicated by I/V curves of evoked $EPSC_{NMDAR}$ (**Fig. 1j**) were not altered in GluA1^{C2KI} or GluA2^{C1KI} mice. Finally, presynaptic function as assessed by paired-pulse facilitation (PPF) was unaffected in these mice (**Fig. 1k**,**l**). Taken together, these results indicate that the CTD replacements in GluA1^{C2KI} and GluA2^{C1KI} mice did not significantly alter basal synaptic function, receptor assembly, subunit composition or channel properties of AMPARs. Therefore, these new mice constitute greatly improved models to specifically address the role of the CTDs of endogenous AMPARs in synaptic plasticity.

Impaired LTP, but intact LTD, in GluA1^{C2KI} mice

To determine the role of the CTD of GluA1 in synaptic plasticity, we compared LTP and LTD at CA1 synapses between WT and GluA1^{C2KI} mice. As show in **Fig. 2a**, delivery of high frequency stimulation (HFS, 100 pulses at 100 Hz) induced a persistent increase in fEPSP in WT, but this LTP was completely abolished in GluA1^{C2KI} mice. To test the possibility that the lack of LTP in GluA1^{C2KI} mice might be due to an impaired threshold for LTP induction, we applied multiple trains of HFS (4 trains with 10 s inter-train interval) but, as shown in **Fig. 2b**, while this protocol produced stable LTP in WT, it failed to induce any LTP in GluA1^{C2KI} mice. We also employed a spaced induction protocol where each of the four 100 Hz trains was separated by a 5 min inter-train interval, and found that LTP was significantly reduced in GluA1^{C2KI} mice (**Fig. 2c**). To ascertain whether the LTP induced by HFS was dependent on the activation of NMDARs, we induced LTP in the presence of D-2-amino-5-phosphonopentanoic acid (AP5) (100 μM) and found that LTP was completed blocked (**Fig. 2d)**. In contrast to the impaired LTP, LTD induced by low frequency stimulation (LFS, 900 pulses at 1 Hz for field recordings and 900 pulses at 5 Hz at -40 mV for whole-cell recordings) was indistinguishable between WT and GluA1^{C2KI} mice (**Fig. 2e**). To investigate whether the LTD induced by the LFS protocol was dependent on the activation of NMDARs, we perfused 100 μM AP5 10 min before and during the induction protocol, and this completely blocked LTD in both WT and GluA1^{C2KI} mice (**Fig. 2f**). Consistent with this NMDAR-dependence, application of MPEP (10 μM), a specific antagonist for mGluR5, had no effect on LTD in WT or GluA1^{C2KI} mice (**Fig. 2g**). These results indicate that the CTD of GluA1 is essential for NMDAR-dependent LTP, but not for NMDAR-LTD.

Absence of LTD, but enhanced LTP, in GluA2^{C1KI} mice

To determine the role of the CTD of GluA2 in synaptic plasticity, we compared LTP and LTD at the CA1 synapse between WT and GluA2^{C1KI} mice. As shown in **Fig. 3a**, delivery of LFS (900 pulses at 1 Hz) induced stable LTD of fEPSPs in WT, but not in GluA2^{C1KI} mice. Similarly, delivery of LFS (900 pulses at 5 Hz at -40 mV) in whole cell recordings generated LTD in WT, but not in GluA2^{C1KI} mice (**Fig. 3b**). To investigate whether the LTD induced by the LFS protocol was dependent on the activation of NMDARs, we again tested the effect of AP5 (100 μM) and MPEP (10 μM). As shown in **Fig. 3c**,**d**, AP5, but not MPEP, blocked LTD in WT mice. As expected, neither drugs had any effect in GluA2^{C1KI} mice (i.e. where LTD was absent). In contrast to the impaired LTD, LTP was readily induced in GluA2^{C1KI} mice. In fact, the magnitude of LTP induced by HFS (100 pulses at 100 Hz) was higher in GluA2^{C1KI} mice compared to the WT control (**Fig. 3e**). In GluA2 KO mice, there was enhanced LTP due to the presence of an additional component of LTP that is dependent on Ca^{2+}-permeable AMPARs rather than NMDARs[19]. In contrast, in the GluA2^{C1KI} mice, LTP was completely blocked by AP5 (**Fig. 3f**). In conclusion, these results demonstrate that the CTD of GluA2 is essential for NMDAR-dependent LTD, but not for NMDAR-dependent LTP.

Intact mGluR-LTD in GluA2^{C1KI} and GluA1^{C2KI} mice

At the CA1 synapse, mGluR-LTD coexists with NMDAR-LTD. Although distinct in the induction mechanisms, both forms of LTD appear to involve the removal of AMPARs from the synapse[2,30,31]. However, whether or not the mechanisms used to remove these receptors are the same is unknown. Therefore, we examined whether GluA2^{C1KI} mice are also impaired in mGluR-LTD. As shown in **Fig. 3g**, delivery of paired-pulse low frequency stimulation (PP-LFS, 900 pairs of pulses at 1 Hz with 50 ms pairing interval), a widely used protocol to induce mGluR-LTD[32], resulted in an indistinguishable amount of LTD between WT and GluA2^{C1KI} mice. Similarly, PP-LFS elicited an equal amount of LTD

in WT and GluA1^{C2KI} mice (**Supplementary Fig. S3a**). To ascertain whether the LTD induced by the PP-LFS protocol was indeed mGluR-dependent, we applied either AP5 (100 μM) or MPEP (10 μM). As shown in **Supplementary Fig. S3b**,**c**, PP-LFS induced LTD in all genotypes was completely blocked by MPEP, but not by AP5. Finally, we also induced mGluR-LTD by bath application of the mGluR agonist DHPG (100 μM). As shown in **Fig. 3h**, DHPG induced equal amounts of LTD in WT and GluA2^{C1KI} mice and this DHPG-induced LTD was blocked by MPEP, but not by APV (**Supplementary Fig. S4**). These results indicate that although the CTD of GluA2 is essential for NMDAR-LTD, it is not required for mGluR-LTD.

Restoration of both LTP and LTD in GluA1^{C2KI}/GluA2^{C1KI} double mutant mice

The results so far provide clear evidence that the CTDs of GluA1 and GluA2 are necessary for NMDAR-LTP and NMDAR-LTD, respectively, but are these domains within a receptor sufficient? To address this question, we examined LTP and LTD in GluA1^{C2KI}/GluA2^{C1KI} double CTD replacement mice. In these mice, both CTDs of GluA1 and GluA2 are present in the receptor complex, but they are linked to different receptor subunits. If the CTD of GluA1 and GluA2 is the sole determinant within the receptor for LTP and LTD, respectively, then one would expect that both LTP and LTD would be restored in the double mutant mice. As shown in **Fig. 4a**, delivery of HFS (100 pulses at 100 Hz) generated an indistinguishable amount of LTP in WT and GluA1^{C2KI}/GluA2^{C1KI} mice. Similarly, delivery of 4 trains of HFS (10 s inter-train interval) also resulted in the same amount of LTP in WT and GluA1^{C2KI}/GluA2^{C1KI} mice (**Fig. 4b**). In addition, delivery of LFS (900 pulses at 1 Hz) generated a similar amount of LTD in WT and GluA1^{C2KI}/GluA2^{C1KI} mice in both field (**Fig. 4c**) and whole cell recordings (**Fig. 4d**). Therefore, the LTP deficit in GluA1^{C2KI} mice and LTD deficit in GluA2^{C1KI} mice were completely rescued to WT levels in the double CTD replacement mice. These results confirm that

the CTDs are the sufficient domains of GluA1 and GluA2 for specifying LTP and LTD expression, respectively, revealing the dominant role of the CTDs in governing bidirectional synaptic plasticity.

Impaired synaptic delivery and removal of AMPARs in GluA1^{C2KI} and GluA2^{C1KI} mice, respectively

To further elucidate the mechanisms underlying the LTP and LTD deficits in GluA1^{C2KI} and GluA2^{C1KI} mice, we examined the trafficking behavior of AMPARs. First, we examined dendritic spines and surface AMPARs in cultured hippocampal neurons under basal conditions. As shown in **Supplementary Fig. S5a-c**, no differences were found in either spine density or spine length between WT, GluA1^{C2KI} and GluA2^{C1KI} mice. The level of basal surface (**Supplementary Fig. S5d**,**e**) and total AMPARs (**Supplementary Fig. S5f**) also showed no differences between WT and GluA1^{C2KI} neurons. The amount of basal surface AMPARs assessed using an antibody directed to the CTD of GluA2 (**Supplementary Fig. S5d**,**e**) was lower in GluA2^{C1KI} neurons although total AMPARs in these neurons were similar to WT (**Supplementary Fig. S5f**). The total amount of the presynaptic marker synaptophysin was not altered in either GluA1^{C2KI} or GluA2^{C1KI} neurons (**Supplementary Fig. S5g**).

To examine the activity-dependent AMPAR surface/synaptic delivery, we analyzed the amount of total surface and synaptic GluA2 with or without glycine treatment (200 μM, 3 min), a protocol known to induce AMPAR surface insertion in cultured hippocampal neurons[33]. In WT neurons, glycine treatment resulted in a significant increase in both total surface and synaptic GluA2 and these glycine-induced changes in GluA2 were blocked by AP5 (**Fig. 5a**,**d**). However, in neurons from GluA1^{C2KI} neurons, glycine treatment did not affect either total surface or synaptic GluA2 (**Fig. 5b,e**). In contrast to GluA1^{C2KI} neurons, glycine treatment of GluA2^{C1KI} neurons induced a significant increase in both

total surface and synaptic GluA2 (**Fig. 5c**,**f**), similar to WT neurons. Therefore, the activity-dependent AMPAR insertion induced by glycine is defective in GluA1^{C2KI}, but not in GluA2^{C1KI}, neurons.

To examine the activity-dependent AMPAR removal from the synapse, we treated cultured hippocampal neurons with NMDA (25 μM, 3 min) to trigger endocytosis of AMPARs. As shown in **Fig. 5g,j**, NMDA treatment resulted in a significant decrease in both total surface and synaptic GluA2 and this NMDA-induced decrease in GluA2 was blocked by AP5. In GluA1^{C2KI} neurons, NMDA treatment induced a similar decrease in both total surface and synaptic GluA2, which was also dependent on activation of NMDARs (**Fig. 5h**,**k**). However, in GluA2^{C1KI} neurons, NMDA treatment did not trigger any changes in either total surface or synaptic GluA2 (**Fig. 5i,l**). Therefore, GluA2^{C1KI}, but not GluA1^{C2KI} neurons, are defective in NMDA induced endocytosis of AMPARs.

To extend the results from cultured neurons to a more physiological condition, we examined surface AMPARs on acute hippocampal slice treated with glycine (200 μM, 3 min) or NMDA (25 μM, 3 min). First, we performed biotinylation experiments to examine total surface AMPARs. As shown in **Fig. 6a-f** and **Supplementary Fig. S8**, glycine induced an increase in surface GluA2 in WT and GluA2^{C1KI}, but not in GluA1^{C2KI} slices, whereas NMDA induced a decrease in surface GluA2 in WT and GluA1^{C2KI}, but not in GluA2^{C1KI} slices. To further determine whether synaptic AMPARs were affected in a similar fashion, we conducted immunohistochemical staining of fixed hippocampal slices after the treatment. As shown in **Fig. 6g-m**, similar results were obtained, that is, glycine treatment caused an increase in both total surface and synaptic GluA2 in WT and GluA2^{C1KI}, but not in GluA1^{C2KI} slices, whereas NMDA treatment resulted in a decrease in total surface and synaptic GluA2 in WT and GluA1^{C2KI}, but not in GluA2^{C1KI} slices.

Taken together these results are consistent with the hypothesis that the CTDs of GluA1 and GluA2 are essential for activity-dependent AMPAR trafficking and suggest that the LTP deficit in GluA1^{C2KI} mice and the LTD deficit GluA2^{C1KI} mice are caused by defective AMPAR delivery and removal, respectively.

An increase in single channel conductance in WT and GluA2^{C1KI}, but not in GluA1^{C2KI} mice following LTP induction.

To further investigate the mechanisms by which the CTDs impact LTP, we analyzed single channel conductance (γ) of synaptic AMPARs. Previous studies suggest that an increase in γ occurs in some neurons undergoing LTP[34], but the receptor subunits and domains involved are unknown. Therefore, we performed whole cell recordings and estimated γ, before and after LTP induction (4 trains of 100 Hz with 10 s inter-train intervals) using peak-scaled, non-stationary fluctuation analysis[34]. As shown in **Fig. 7a-c**, LTP was induced in WT and GluA2^{C1KI}, but not in GluA1^{C2KI} mice, consistent with the results obtained from field potential recordings. During baseline recordings, the averaged γ showed no differences between genotypes (**Fig. 7d-h**), suggesting that the CTDs of GluA1 and GluA2 do not differentially impact γ of synaptic AMPARs under basal conditions. However, after LTP induction, WT and GluA2^{C1KI}, but not GluA1^{C2KI} neurons showed a significant increase in γ compared to baseline (**Fig. 7d-h**). These results indicate that the CTD of GluA1, but not of GluA2, is required for an increased γ after LTP induction. Other channel properties such as the rise and decay time of EPSCs were not altered after the LTP induction protocol in all three genotypes (**Fig. 7i,j**).

Distinct deficits in spatial and fear memory in GluA1^{C2KI} and GluA2^{C1KI} mice

The generation of these new mice that have pronounced yet specific deficits in hippocampal LTP and LTD provides useful models for relating these forms of synaptic plasticity to learning and memory. First, we used an open-field test to assess locomotor activity. The GluA1^{C2KI} and GluA2^{C1KI} mice were similar to WT mice on most measures, except that the GluA1^{C2KI} mice were slightly more active (**Supplementary Fig. S6a**,**b**). Second, we used an elevated plus maze to evaluate the emotional state and anxiety levels but found no significant differences between genotypes (**Supplementary Fig. S6c**,**d**).

To examine their cognitive performance, we first conducted the visible platform version of the Morris water maze (MWM) test (**Supplementary Fig. S7a**), and showed that WT, GluA1^{C2KI} and GluA2^{C1KI} mice performed equally well, suggesting that swim ability, motivation and visual acuity were comparable in WT, GluA1^{C2KI} and GluA2^{C1KI} mice. To assess spatial learning and memory, we performed the hidden platform water maze test. As shown in **Fig. 8a**, during the learning acquisition phase, although GluA2^{C1KI} mice showed no differences from WT, the GluA1^{C2KI} mice were significantly slower to learn the task. To assess the memory, we carried out probe tests 2 h and 24 h after the training. As shown in **Fig. 8b** (2 h) and **Fig. 8c** (24 h), both WT and GluA2^{C1KI} mice, but not GluA1^{C2KI} mice, spent significantly more time in the target zone compared to other zones. Similar results were obtained when the target quadrant was analyzed (**Supplementary Fig. 7b,c)**. To determine whether the deficits in GluA1^{C2KI} mice could be related to the differences in training paradigm, we modified the protocol by increasing the duration and intensity of the training, but found that GluA1^{C2KI} mice were still impaired in both learning and memory tests (**Fig. 8d-f; Supplementary Fig. 7d,e**). These results indicate that the CTD of GluA1, but not of GluA2, is critical for spatial learning and memory.

To assess contextual memory, we used the fear conditioning paradigm. As shown in **Fig. 8g**, during the training session all three genotypes responded to electric foot shocks equally well. During the contextual test carried out 2 h (**Fig. 8h**) or 24 h (**Fig. 8i**) after the training, GluA2^{C1KI} mice, but not

GluA1^{C2KI} mice, showed a significantly reduced freezing compared to the WT control. In the following cued tests, all three genotypes showed similar freezing in response to the tone (**Supplementary Fig. S7f**,g), suggesting that the fear response to simple conditioning stimulus remains intact in these mice. The deficits in GluA2^{C1KI} mice but not in GluA1^{C2KI} mice in contextual fear conditioning was surprising because several previous studies have shown that both GluA1 and LTP are involved in fear contextual memory[7,35-37]. We considered the possibility that the three-shock training might have been too strong to reveal an effect in GluA1^{C2KI} mice. We therefore decreased the numbers of electric foot shocks from three to two. As shown in **Fig. 8j-l**, although GluA1^{C2KI} showed reduced freezing at 2 h after the training, no difference was found at 24 h after the training compared to WT mice. The GluA2^{C1KI} mice remained impaired at both intervals. Interestingly, in cued tests, GluA1^{C2KI} mice showed some mild deficits (**Supplementary Fig. S7h,i**). We also used another fear conditioning paradigm that is thought to be particularly sensitive to pre-training hippocampal damage[38]. In this version of the test, mice were pre-exposed to the conditioning chamber in the absence of any shocks for 4 min. The next day, mice were placed back in the chamber and immediately received shocks. The mice were then tested 24 h later for a freezing responses. As shown in **Fig. 8m**, the GluA2^{C1KI}, but not GluA1^{C2KI} mice showed significant impairments. These results indicate that the CTD of GluA2 is likely more important than, but do not exclude a role for, the CTD of GluA1 in contextual fear memory.

DISCUSSION

In this study, we have created new mouse strains where the CTDs of the endogenous AMPARs are switched. These mice have allowed us, for the first time, to address the *in vivo* role of the CTDs of AMPARs in LTP and LTD without affecting the formation of heteromeric receptor complexes, their ion channel properties or basal synaptic strength. We reveal that the CTDs of GluA1 and GluA2 are

necessary and sufficient for NMDAR-LTP and LTD, respectively, and confer specific effects on distinct forms of learning and memory.

Unlike the traditional GluA mouse models, which are defective in both AMPAR expression and properties[9,10,19-21,23], GluA1^{C2KI} or GluA2^{C1KI} mice exhibit little changes in these parameters. The interpretation is that the CTD replacements have no effects on receptor expression or assembly, allowing the formation of physiologically normal, heteromeric AMPARs. These results are consistent with *in vitro* studies showing that GluA1 or GluA2 homomers are defective in receptor assembly and ER exit and this is mediated by the extracellular N-terminal domain (NTD) and transmembrane Q/R segment of the receptor[22]. Thus, the unique features of the CTD specific to GluA1 or of GluA2 do not appear to differentially impact the channel properties of AMPARs or synaptic strength under basal conditions. It is interesting to note however, that although basal synaptic responses are not altered, the level of total surface GluA2 is lower in GluA2^{C1KI} neurons. One possibility is that GluA2^{C1KI} receptors may behave more like GluA1 in terms of regulated membrane recycling leading to accumulation in recycling endosomes, which could explain lower basal surface levels as well as enhanced LTP in these mice.

Previous studies using exogenously expressed mutant subunits in cultured hippocampal slices have suggested that the CTD of GluA1, but not of GluA2, is critical for LTP expression[5-7,12,13]. However, this approach has been questioned due to the abnormally high level of the recombinant receptors and the formation of non-physiological homomeric receptors. In addition, these studies did not directly address the role of native AMPARs. The use of GluA1^{C2KI} and GluA2^{C1KI} mice overcomes these problems. In GluA1^{C2KI}, but not GluA2^{C1KI} mice, LTP induced by HFS is absent confirming, in a more direct manner, that the CTD of GluA1, but not of GluA2, is essential for this form of LTP. The lack of LTP in GluA1^{C2KI} mice is not likely due to the inadequate activation of NMDARs during the induction phase

because the expression of NMDARs and their channel properties are unaltered in these mice. The observations that both the activity-dependent synaptic delivery and an increase in single channel conductance of AMPARs are impaired in GluA1^{C2KI}, but not GluA2^{C1KI} mice, support the idea that direct modifications of AMPARs underlie LTP expression. Our results are consistent with fact that the CTD of GluA1 contains motifs for phosphorylation (e.g., Ser831 and Ser845) and protein-protein interactions, both of which play critical roles in AMPAR trafficking and modifications of channel conductance[39]. Previous studies have shown that GluA1 KO mice are impaired in LTP[10,20], but this effect is complicated by the formation of the non-physiological receptors and a reduction in the surface AMPARs[9,10,23]. It is interesting to note that LTP is intact or only mildly affected in mice with an altered PDZ domain[28] or phosphorylation sites (Ser831 and Ser845) at the CTD of GluA1[27], suggesting that there are multiple, independent mechanisms operating within this domain and their combined action may be necessary for the full expression of LTP. Consistent with this, there are numerous additional post-translational modification sites identified at the CTD of GluA1[39].

In GluA2^{C1KI}, but not in GluA1^{C2KI} mice, LTD induced by LFS is absent, indicating that the CTD of GluA2, but not of GluA1, is essential for LTD. Although the involvement of GluA2 in LTD has been previously suggested using peptides targeting the GluA2 CTD protein interactions[14-18,40], the potential off-target effects of these peptides complicate the validity of the conclusion. In addition, GluA2 KO or conditional mutant mice lacking all major AMPAR subunits (GluA1-3) are capable of LTD expression[11,19,21], apparently refuting the requirement for GluA2 in LTD. However, these mouse models are also compromised by dramatic changes in basal synaptic function as well as AMPARs properties, particularly enhanced Ca^{2+} permeability. Therefore, the use of GluA2^{C1KI} mice that have no changes in these basal properties but complete absence of LTD conclusively establishes the indispensable role of

the CTD of GluA2 in LTD. The fact that NMDA-induced AMPAR removal from the synapse is impaired in these mice strongly supports that the CTD of GluA2 enables LTD through activity-dependent endocytosis of AMPARs. It is intriguing to note that although NMDAR-LTD is absent in GluA2^{C1KI} mice, mGluR-LTD remains intact in both GluA2^{C1KI} and GluA1^{C2KI} mice, suggesting that mGluR-LTD is independent of the CTDs of GluA1 or GluA2. Previous studies have shown that although the induction mechanisms of mGluR-LTD and NMDAR-LTP are different, the expression of both forms of LTD requires, at least in part, the removal of AMPARs from the synapse[30,31]. Therefore, different domains of AMPARs must be involved in mGluR-LTD**.**

Another key finding of this study is that the CTDs of GluA1 and GluA2 are not only necessary, but also sufficient domains within AMPARs for determining the directionality of synaptic plasticity. Although the CTDs of AMPARs have been extensively investigated, none of the previous studies were able to address whether these domains can exert dominant effects over the rest of the receptor. Our results that both LTP and LTD are restored in the CTD swapped mutant mice, indicating that the CTDs of GluA1 and GluA2 can confer their specific effects on LTP and LTD, respectively, regardless of whether they are a part of GluA1 or GluA2. However, this does not mean that the CTD of AMPARs alone is sufficient for LTP or LTP expression.

Finally, our results have revealed that the CTDs of GluA1 and GluA2 play distinct roles in learning and memory. Previous studies have shown that GluA1 KO or KI mice are not impaired in either learning acquisition or reference memory[20,27,41,42], but it is possible that the altered basal transmission in these mice may have caused functional compensations. It is also of concern that these previous mouse models have a hybrid genetic background, which could affect the behavioral performance. In the case of GluA2

KO mice, learning and memory tests have not been possible due to their growth retardation and motor deficits[19,29]. The GluA1^{C2KI} and GluA2^{C1KI} mice, which do not have these caveats, allow learning processes to be addressed more definitively. In the water maze test, both learning acquisition and memory are impaired in GluA1^{C2KI}, but not GluA2^{C1KI} mice. These impairments are not likely related to training procedures because longer training does not mitigate the deficits. Therefore, the present study provides strong evidence for a critical role of native GluA1 in spatial learning and memory, and is consistent with a role for GluA1-dependent LTP in this form of memory. Compared to spatial performance, contextual fear memory, as assessed by several different paradigms, is less affected in GluA1^{C2KI} mice. These results appear inconsistent with previous studies demonstrating the involvement of LTP in fear memory[7,35-37] and suggest a dissociation between spatial and contextual fear memory. It is possible however that when hippocampal LTP is impaired, other brain regions[43] may compensate and enable contextual, but not spatial learning, because the latter is more demanding and requires a precise memory of the platform location. Previous studies have indeed shown that hippocampal damage prior to training, which is in principle similar to the current genetic manipulations, impairs spatial learning in the water maze[44], but has only mild effects on contextual fear learning[45,46]. Damage to the parahippocampal regions (e.g., entorhinal cortex) impairs contextual, but not spatial learning[47], suggesting that corticohippocampal circuits are differentially involved in spatial and contextual memories. Therefore, it would be interesting to investigate LTP in extra-hippocampal brain regions in GluA1^{C2KI} mice. Another interesting finding of the study is that, in clear contrast to GluA1^{C2KI} mice, GluA2^{C1KI} mice are impaired in contextual, but not spatial performance, suggesting a role for LTD in fear memory. A previous study shows that KO mice deficient in Bax, a member of the Bcl-2 family involved in apoptotic cell death, are impaired in hippocampal LTD and fear memory, but these mice also suffer from other behavioral deficits that undermine a link between the fear memory and LTD deficit[48]. Our results that GluA2^{C1K}

mice are impaired in NMDAR-LTD and contextual fear memory without other behavioral deficits, strongly support a role for NMDAR-LTD in this form of memory. Thus, LTP and LTD differentially contribute to spatial and contextual memory.

Acknowledgements:

This work was supported by grants from the Canadian Institutes of Health Research (CIHR, MOP119421, ZPJ; FDN154276, GLC), Canadian Natural Science and Engineering Research Council (NSERC, RGPIN341498, ZPJ), Natural Science Foundation of China (NSFC 31571040, ZZ), NSFC and CIHR Joint Health Research Initiative Program (81161120543, WX and CCI117959, ZPJ), Brain Canada (ZPJ and GLC) and the Hospital for Sick Children Foundation (ZPJ). SX was supported by the Scientific Research Foundation of Graduate School of Southeast University, China. We thank Yu-Tian Wang for GluA2-CTD antibodies, Wei Lu for the use of the fear conditioning chambers, Lifang Han, Rui Mao and other members of Jia lab for their technical assistance and comments on the manuscript.

Author Contribution:

ZPJ conceived and supervised the study. AL, GLC and ZPJ designed the experiments. ZZ, AL, SX, CL, JQ and YM performed experiments. ZZ, AL, SX, CL, PP and WX analyzed data. ZPJ, GLC and AL wrote the paper. All authors read and approved the final manuscript.

Competing Financial Interests Statement:

The authors declare that they do not have any competing financial interests.

References:

1. Bliss, T. V. P. & G. L. Collingridge, G. L. A synaptic model of memory: long-term potentiation in the hippocampus. *Nature* **361**, 31-39 (1993).
2. Malenka, R. C. & Bear, M. F. LTP and LTD: an embarrassment of riches. *Neuron* **44**, 5-21 (2004).
3. Kandel, E. R., Dudai, Y. & Mayford, M. The molecular and systems biology of memory. *Cell* **157**, 163-186 (2014).
4. Henley, J. M. & Wilkinson, K. A. Synaptic AMPA receptor composition in development, plasticity and disease. *Nat. Rev. Neurosci.* **17**, 337-350 (2016).
5. Malinow, R. & Malenka, R. C. AMPA receptor trafficking and synaptic plasticity. *Annu. Rev. Neurosci.* **25**, 103-126 (2002).
6. Collingridge, G. L., Isaac, J. T. & Wang, Y. T. Receptor trafficking and synaptic plasticity. *Nat. Rev. Neurosci.* **5**, 952-962 (2004).
7. Kessels, H. W. & Malinow, R. Synaptic AMPA receptor plasticity and behavior. *Neuron* **61**, 340-350 (2009).
8. Huganir, R. L. & Nicoll, R.A. AMPARs and synaptic plasticity: the last 25 years. *Neuron* **80**, 704-717 (2013).
9. Lu. L. *et al.* Subunit composition of synaptic AMPA receptors revealed by a single-cell genetic approach. *Neuron* **62**, 254-268 (2009).
10. Granger, A. J. *et al.* LTP requires a reserve pool of glutamate receptors independent of subunit type. *Nature* **493**, 495-500 (2013).
11. Granger, A. J. & Nicoll, R. A LTD expression is independent of glutamate receptor subtype. *Front.Synaptic Neurosci.* **6**, 15 (2014).
12. Hayashi, Y. *et al.* Driving AMPA receptors into synapses by LTP and CaMKII: requirement for GluR1 and PDZ domain interaction. *Science* **287**, 2262-2267 (2000).
13. Shi, S. H., Hayashi, Y., Esteban, J. A. & R. Malinow, R. Subunit-specific rules governing AMPA receptor trafficking to synapses in hippocampal pyramidal neurons. *Cell* **105**, 331-343 (2001).
14. Nishimune, A. *et al.* NSF binding to GluR2 regulates synaptic transmission. *Neuron* **21**, 87-97 (1998).
15. Lüthi, A. *et al.* Hippocampal LTD expression involves a pool of AMPARs regulated by the NSF-GluR2 interaction. *Neuron* **24**, 389-399 (1999).
16. Lüscher, C. *et al.* Role of AMPA receptor cycling in synaptic transmission and plasticity. *Neuron* **24**, 649-658 (1999).
17. Lee, S. H., Liu, L., Wang, Y. T. & Sheng, M. Clathrin adaptor AP2 and NSF interact with overlapping sites of GluR2 and play distinct roles in AMPA receptor trafficking and hippocampal LTD. *Neuron* **36**, 661-674 (2002).
18. Ahmadian, G *et al.* Tyrosine phosphorylation of GluR2 is required for insulin-stimulated AMPA receptor endocytosis and LTD. *EMBO J.* **23**, 1040-1050 (2004).
19. Jia Z. *et al.* Enhanced LTP in mice deficient in the AMPA receptor GluR2. *Neuron* **17**, 945-956 (1996).
20. Zamanillo, D. *et al.* Importance of AMPA receptors for hippocampal synaptic plasticity but not for spatial learning. *Science* **284**, 1805-1811 (1999).
21. Meng, Y., Zhang, Y. & Jia, Z. Synaptic transmission and plasticity in the absence of AMPA glutamate receptor GluR2 and GluR3. *Neuron* **39**, 163-176 (2003).

22. Greger, I. H. Ziff, E. B. & Penn, A. C. Molecular determinants of AMPA receptor subunit assembly. *Trends Neurosci.* **30**, 407-416 (2007).
23. Andrásfalvy, B. K. et al. Magee, Impaired regulation of synaptic strength in hippocampal neurons from GluR1-deficient mice. *J Physiol.* **552**, 35-45 (2003).
24. Sans, N. *et al.* Aberrant formation of glutamate receptor complexes in hippocampal neurons of mice lacking the GluR2 AMPA receptor subunit. *J. Neurosci.* **23**, 9367-9373 (2003).
25. Plant, K. *et al.* Transient incorporation of native GluR2-lacking AMPA receptors during hippocampal long-term potentiation. *Nat. Neurosci.* **9**, 602-604 (2006).
26. Liu, S. J. & Zukin, R. S. Ca2+-permeable AMPA receptors in synaptic plasticity and neuronal death. *Trends Neurosci.* **30**, 126-134 (2007).
27. Lee, H. K. *et al.* Phosphorylation of the AMPA receptor GluR1 subunit is required for synaptic plasticity and retention of spatial memory. *Cell* **112**, 631-643 (2003).
28. Kim, C. H. *et al.* Persistent hippocampal CA1 LTP in mice lacking the C-terminal PDZ ligand of GluR1. *Nat. Neurosci.* **8**, 985-987 (2005).
29. Gerlai, R., Henderson, J. T., Roder, J. & Jia, Z. Multiple behavioral anomalies in GluR2 mutant mice exhibiting enhanced LTP. *Behav. Brain Res.* **95**, 37-45 (1998).
30. Collingridge, G.L., Peineau, S., Howland, J. G. & Wang, Y. T. Long-term depression in the CNS. *Nat. Rev. Neurosci.* **11**, 459-473 (2010).
31. Lüscher, C. & Huber, K. M. Group 1 mGluR-dependent synaptic long-term depression (mGluR-LTD): mechanisms and implications for circuitry & disease. *Neuron* **65**, 445-459 (2010).
32. Kemp, N., Mcqueen, J., Faulkes, S. & Bashir, Z. I. Different forms of LTD in the CA1 region of the hippocampus: role of age and stimulus protocol. *Eur. J. Neurosci.* **12**, 360-366 (2000).
33. Lu, W. *et al.* Activation of synaptic NMDA receptors induces membrane insertion of new AMPA receptors and LTP in cultured hippocampal neurons. *Neuron* **29**, 243-254 (2001).
34. Benke, T.A., Lüthi, A., Isaac, J.T. & Collingridge, G.L. Modulation of AMPA receptor unitary conductance by synaptic activity. *Nature* **393**, 793-797 (1998).
35. Clem, R.L. & Huganir, R.L. Calcium-permeable AMPA receptor dynamics mediate fear memory erasure. *Science* **330**, 1108-1112 (2010).
36. Humeau, Y. *et al.* A pathway-specific function for different AMPA receptor subunits in amygdala long-term potentiation and fear conditioning. *J. Neurosci.* **27**, 10947-10956 (2007).
37. Mitsushima, D. *et al.* Contextual learning requires synaptic AMPA receptor delivery in the hippocampus. *Proc Natl Acad Sci USA* **108**, 12503-12508 (2011).
38. Rudy, J.W., Barrientos, R.M. & O'Reilly, R.C. Hippocampal formation supports conditioning to memory of a context. B*ehav Neurosci.* **116,** 530-538 (2002).
39. Lu, W. & Roche, K. W. Posttranslational regulation of AMPA receptor trafficking and function. *Curr. Opin. Neurobiol.* **22**, 470-479 (2012).
40. Kim, C.H.,Chung, H. J., Lee, H. K. & Huganir, R. L. Interaction of the AMPA receptor subunit GluR2/3 with PDZ domains regulates hippocampal long-term depression. *Proc. Natl. Acad. Sci. USA* **98**, 11725-11730 (2001).
41. Reisel, D. *et al.* Spatial memory dissociations in mice lacking GluR1. *Nat. Neurosci.* **5**, 868-873 (2002).
42. Schmitt, W. B. *et al.* Spatial reference memory in GluR-A-deficient mice using a novel hippocampal-dependent paddling pool escape task. *Hippocampus* **14**, 216-223 (2004).

43. Bannerman, D.M. et al. Hippocampal synaptic plasticity, spatial memory and anxiety. *Nat Rev Neurosci.* **15**, 181-192 (2014).
44. Moser, E., Moser, M.B. & Andersen, P. Spatial learning impairment parallels the magnitude of dorsal hippocampal lesions, but is hardly present following ventral lesions. *J Neurosci.* **13**, 3916-3925 (1993).
45. Frankland, P.W. *et al*. The dorsal hippocampus is essential for context discrimination but not for contextual conditioning. *Behav Neurosci*. **112**, 863-874 (1998).
46. Wiltgen, B.J. *et al.* Context fear learning in the absence of the hippocampus. *J Neurosci*. **26**, 5484-5491 (2006).
47. Burwell, R.D., Saddoris, M.P., Bucci, D.J. & Wiig, K.A. Corticohippocampal contributions to spatial and contextual learning. *J Neurosci.* **24**, 3826-3836 (2004).
48. Liu, X., Gu, Q. H., Duan, K. & Li, Z. NMDA receptor-dependent LTD is required for consolidation but not acquisition of fear memory. *J. Neurosci.* **34**, 8741-8748 (2014).

Figure Legend:

Fig. 1. Basal synaptic and AMPAR properties in GluA1^{C2KI} and GluA2^{C1KI} mice.

(**a**) Amino acid sequences of the CTDs of GluA1 and GluA2 that are replaced or swapped in GluA1^{C2KI}, GluA2^{C1KI} and GluA1^{C2KI}/GluA2^{C1KI} mice. (**b**) Predicted AMPAR subunit composition in WT, GluA1^{C2KI}, GluA2^{C1KI} and GluA1^{C2KI}/GluA2^{C1KI} mice. In GluA1^{C2KI} mice, the CTD of GluA1 is replaced by that of GluA2; in GluA2^{C1KI} mice, the CTD of GluA2 is replaced by that of GluA1; in GluA1^{C2KI}/GluA2^{C1KI} double mutant mice, the CTD of GluA1 and GluA2 is swapped. (**c**) Normal input/output curve of fEPSPs in GluA1^{C2KI} mice (at 0.1 mA stimulus: WT_{pre} = 0.00 ± 0.01 mV, WT_{fEPSP} = 0.13 ± 0.02 mV, GluA1$^{C2KI}{}_{pre}$ = 0.00 ± 0.02 mV, GluA1$^{C2KI}{}_{fEPSP}$ = 0.14 ± 0.03 mV; at 0.2 mA stimulus: WT_{pre} = 0.03 ± 0.02 mV, WT_{fEPSP} = 0.30 ± 0.05 mV, GluA1^{C2KI}pre = 0.04 ± 0.02 mV, GluA1$^{C2KI}{}_{fEPSP}$ = 0.36 ± 0.09 mV; at 0.3 mA stimulus: WT_{pre} = 0.09 ± 0.02 mV, WT_{fEPSP} = 0.61 ± 0.10 mV, GluA1^{C2KI}pre = 0.13 ± 0.03 mV, GluA1$^{C2KI}{}_{fEPSP}$ = 0.71 ± 0.15 mV; at 0.4 mA stimulus: WT_{pre} = 0.15 ± 0.03 mV, WT_{fEPSP} = 0.83 ± 0.11 mV, GluA1^{C2KI}pre = 0.20 ± 0.04 mV, GluA1$^{C2KI}{}_{fEPSP}$ = 0.89 ± 0.16 mV. WT: n = 7 slices from 4 mice; GluA1^{C2KI}: n = 7 slices from 4 mice). Scale bar: 0.5 mV/20 ms.

(**d**) Normal input/output curve of fEPSPs in GluA2^{C1KI} mice (at 0.1 mA stimulus: WT_{pre} = 0.04 ± 0.00 mV, WT_{fEPSP} = 0.13 ± 0.03 mV, GluA2^{C1KI}pre = 0.03 ± 0.00 mV, GluA2$^{C1KI}{}_{fEPSP}$ = 0.10 ± 0.02 mV; at 0.2 mA stimulus, WT_{pre} = 0.10 ± 0.02 mV, WT_{fEPSP} = 0.28 ± 0.06 mV, GluA2^{C1KI}pre = 0.06 ± 0.01 mV, GluA2$^{C1KI}{}_{fEPSP}$ = 0.22 ± 0.03 mV; at 0.3 mA stimulus: WT_{pre} = 0.16 ± 0.04 mV, WT_{fEPSP} = 0.51 ± 0.07 mV, GluA2$^{C1KI}{}_{pre}$ = 0.09 ± 0.02 mV, GluA2$^{C1KI}{}_{fEPSP}$ = 0.37 ± 0.05 mV; at 0.4 mA stimulus: WT_{pre} = 0.24 ± 0.04 mV, WT_{fEPSP} = 0.69 ± 0.08 mV, GluA2^{C1KI}pre = 0.15 ± 0.02 mV, GluA2$^{C1KI}{}_{fEPSP}$ = 0.49 ± 0.05 mV; WT: n = 9 slices from 5 mice; GluA2^{C1KI}: n = 9 slices from 5 mice) Scale bar: 0.5 mV/20 ms. (**e**) $EPSC_{NMDAR}/EPSC_{AMPAR}$ ratio in WT (0.83 ± 0.07, n = 23 neurons from 9 mice), GluA1^{C2KI} (0.84 ± 0.17, n = 15 neurons from 6 mice, p = 0.910 compared to WT), GluA2^{C1KI} (0.96 ± 0.14, n = 10 neurons from 6 mice, p = 0.550 compared to WT) and GluA2 KO mice (1.83 ± 0.26, n = 13 neurons from 6 mice, ***p = 0.0001 compared to WT; $F_{(3,57)}$ = 8.751, p = 0.0000726). Scale bar: 50 pA/25 ms. (**f**) Sample traces and summary graphs of whole-cell patch-clamp recordings of mEPSCs of CA1 neurons showing no differences in either frequency (WT = 0.41 ± 0.06 Hz, n = 23 neurons from 14 mice; A1^{C2KI} = 0.35 ± 0.08 Hz, n = 13 neurons from 7 mice; A2^{C1KI} = 0.38 ± 0.08 Hz, n = 11 neurons from 7 mice; $F_{(2, 44)}$ = 0.147, p = 0.863) or amplitude (WT = 14.65 ± 0.49 pA, n = 23 from 14 mice; A1^{C2KI} = 13.25 ± 0.38 pA, n = 13 neurons from 7 mice; A2^{CIKI} = 14.65 ± 1.30 pA, n = 11 neurons from 7 mice; $F_{(2, 44)}$ = 1.224, p = 0.304) between genotypes. Scale bar: 20 pA/1 s. (**g**) Sample traces and summary graph of AMPAR-mediated currents recorded from outside-out patches of CA1 neurons evoked by application of 1 mM glutamate (3 s) showing no differences between genotypes (WT = 367.88 ± 40.85 pA, n = 26 neurons from 7 mice; A1^{C2KI} = 377.01 ± 52.09 pA, n = 21 neurons from 6 mice; A2^{CIKI} = 378.17 ± 62.82 pA, n = 24 neurons from 6 mice; $F_{(2, 68)}$ = 0.012, p = 0.988). Scale bar: 100 pA/5 s. (**h**) Sample traces and summary graph of normalized $EPSC_{AMPAR}$ at various holding potentials showing similar I/V relationships in WT, GluA1^{C2KI} and GluA2^{C1KI} mice, as compared to a strongly rectified I/V curve in

GluA2 KO mice (WT: n = 12 neurons from 7 mice; GluA1^{C2KI}: n = 9 neurons from 5 mice; GluA2^{C1K}: n = 13 neurons from 7 mice; GluA2 KO: n = 9 neurons from 5 mice). Scale bar: 50 pA/25 ms. (**i**) Rectification index of $EPSC_{AMPAR}$ in WT (0.88 ± 0.06, n = 12 neurons from 7 mice), GluA1^{C2KI} (0.78 ± 0.10, n = 9 neurons from 5 mice, p = 0.257 compared to WT), GluA2^{C1KI} (0.83 ± 0.04, n = 13 neurons from 7 mice, p = 0.538 compared WT) and GluA2 KO mice (0.36 ± 0.03, n = 9 neurons from 5 mice, ***p = 0.0000009 compared to WT; $F_{(3, 39)} = 6.041$, p = 0.002). (**j**) Sample traces and summary graph of normalized $EPSC_{NMDAR}$ at various holding potentials showing similar I/V relationships in WT, GluA1^{C2KI} and GluA2^{C1KI} mice. Scale bar: 100 pA/25 ms. (**k**) Normal PPF in GluA1^{C2KI} mice (between genotypes: $F_{(1,13)} = 2.594$, p = 0.131; at 0.025 s: WT = 1.81 ± 0.04, GluA1^{C2KI} = 1.96 ± 0.06; at 0.05 s: WT = 1.80 ± 0.10, GluA1^{C2KI} = 1.93 ± 0.05; at 0.1 s: WT = 1.73 ± 0.08, GluA1^{C2KI} = 1.86 ± 0.05; at 0.2 s: WT = 1.51 ± 0.06, GluA1^{C2KI} = 1.60 ± 0.04; at 0.5 s: WT = 1.25 ± 0.02, GluA1^{C2KI} = 1.24 ± 0.04; at 1 s: WT = 1.12 ± 0.02, GluA1^{C2KI} = 1.15 ± 0.02. WT: n = 7 slices from 7 mice, GluA1^{C2KI}: n = 8 slices from 8 mice). (**l**) Normal PPF in GluA2^{C1KI} mice (between genotypes: $F_{(1,13)} = 0.094$, p = 0.764; at 0.025 s: WT = 1.89 ± 0.10, GluA2^{C1KI} = 1.87 ± 0.11; at 0.05 s: WT = 1.86 ± 0.10, GluA2^{C1KI} = 1.85 ± 0.11; at 0.1 s: WT = 1.81 ± 0.08, GluA2^{C1KI} = 1.85 ± 0.10; at 0.2 s: WT = 1.54 ± 0.04, GluA2^{C1KI} = 1.55 ± 0.06; at 0.5 s: WT = 1.21 ± 0.05, GluA2^{C1KI} = 1.27 ± 0.05; at 1 s: WT = 1.08 ± 0.03, GluA2^{C1KI} = 1.17 ± 0.04. WT: n = 7 slices from 7 mice, GluA2^{C1KI}: n = 8 slices from 8 mice). One-way ANOVA followed by post-hoc Fisher's LSD multiple comparison test for Fig.1e, f, g and i; repeated two-way ANOVA test for Fig.1k,l. Data were presented as mean ± SEM. ***p < 0.001.

Fig. 2. Absence of NMDAR-LTP, but intact NMDAR-LTD in GluA1^{C2KI} mice.

(**a**) Absence of LTP induced by HFS (100Hz, 1s) in GluA1^{C2KI} mice (WT = 120.00 ± 3.21%, n = 5 slices from 5 mice ; A1^{C2KI} = 99.98 ± 3.26%, n = 5 slices from 5 mice; t(8) = 3.092, **p = 0.002). (**b**)

Absence of LTP induced by 4 compressed trains of HFS (with 10 s inter-train intervals) in GluA1^{C2KI} mice (WT = 152.63 ± 13.79%, n = 5 slices from 5 mice; A1^{C2KI} = 108.88 ± 4.44%, n = 6 slices from 6 mice; t(9) = 3.267, **p = 0.010). (**c**) Absence of LTP induced by 4 spaced trains of HFS (with 5 min inter-train intervals) in GluA1^{C2KI} mice (WT = 138.94 ± 6.74%, n = 7 slices from 7 mice; A1^{C2KI} = 106.47 ± 7.50%, n = 7 slices from 7 mice; t(12) = 3.220, **p = 0.007). (**d**) NMDAR-dependence of LTP induced by HSF in WT mice (WT = 163.64 ± 9.80%, n = 5 slices from 5 mice; WT+AP5= 92.08 ± 4.52, n = 5 slices from 5 mice; t(8) = 6.629, ***p = 0.0002). (**e**) Intact LTD in whole cell recordings in GluA1^{C2KI} mice (WT = 55.51 ± 6.22%, n = 4 slices from 4 mice; A1^{C2KI} = 60.26 ± 4.74%, n = 6 slices from 6 mice; t(8) = -0.618, p = 0.554). (**f**) NMDAR-dependence of LTD induced by LFS in WT and GluA1^{C2KI} mice (WT = 105.33 ± 5.97%, n = 5 slices from 5 mice; A1^{C2KI} = 100.33 ± 9.87%, n = 5 slices from 5 mice; t(8) = 0.434, p = 0.676). (**g**) Lack of effect of MPEP on LTD induced by LFS in WT and GluA1^{C2KI} mice **(**WT = 65.45 ± 8.43%, n = 4 slices from 4 mice; A1^{C2KI} = 52.50 ± 3.74%, n = 5 slices from 5 mice; t(7) = 1.518, p = 0.173). Two tailed t-test at 95% confidence interval was used for all bar graphs. Data were presented as mean ± SEM. **p < 0.01, ***p < 0.001. Scale bar: 0.25 mV/25 ms for Fig. 2a-d and 50 pA/25 ms for Fig. 2e-f.

Fig. 3. Absence of NMDAR-LTD, but intact mGluR-LTD in GluA2^{C1KI} mice.

(**a**) Absence of LTD induced by LFS in fEPSP recordings in GluA2^{C1KI} mice (WT = 70.08 ± 3.61%, n = 9 slices from 9 mice; A2^{C1KI} = 102.33 ± 9.38%, n = 9 slices from 9 mice; t(16) = -3.210, **p = 0.005). (**b**) Absence of LTD induced by LFS in whole cell recordings in GluA2^{C1KI} mice (WT = 57.04 ± 4.14%, n = 7 slices from 7 mice; A2^{C1KI} = 95.02 ± 4.77%, n = 7 slices from 7 mice; t(12) = -6.015, ***p = 0.0001). (**c**) NMDAR-dependence of LTD induced by LFS (WT = 87.88 ± 9.89%, n = 5 slices from 5 mice; A2^{C1KI} = 98.97 ± 6.68%, n = 4 slices from 4 mice; t(7) = 0.876, p = 0.410). (**d**) Lack of effect of

MPEP on LTD induced by LFS (WT = 62.06 ± 2.59%, n = 5 slices from 5 mice; A2^{C1KI} = 94.26 ± 8.47%, n = 4 slices from 4 mice; t(7) = 4.027, **p = 0.005). (**e**) Enhanced LTP (4 compressed trains of HFS, with 10 s inter-train intervals) in GluA2^{C1KI} mice (WT = 145.73 ± 5.04%, n = 5 slices from 5 mice; A2^{C1KI} = 196.41 ± 22.27%, n = 6 slices from 6 mice; t(9) = -0.024, p = 0.074). (**f**) NMDAR-dependence of LTP in WT and GluA2^{C1KI} mice (WT+AP5 = 110.16 ± 6.94%, n = 5 slices from 5 mice; A2^{C1KI}+AP5 = 109.89 ± 8.59%, n = 5 slices from 5 mice; t(8) = 0.025, p = 0.981). (**g**) Intact PP-LFS-induced LTD in GluA2^{C1KI} mice (WT = 57.55 ± 7.70%, n = 7 slices from 7 mice; A2^{C1KI} = 54.98 ± 7.42%, n = 8 slices from 8 mice; t(13) = 0.240, p = 0.814). (**h**) Intact DHPG-induced LTD in GluA2^{C1KI} mice (WT = 61.56 ± 2.80%, n = 5 slices from 5 mice; A2^{C1KI} = 59.87 ± 3.47%, n = 5 slices from 5 mice; t(8) = 0.379, p = 0.715). Two tailed t-test at 95% confidence interval was used for all bar graphs. Data were presented as mean ± SEM. **p < 0.01, ***p < 0.001. Scale bar: 0.25 mV/25 ms for Fig. 3a, e and f, and 50 pA/25 ms for Fig. 3b-d, g and h.

Fig. 4. Restoration of both LTP and LTD in GluA1^{C2KI}/GluA2^{C1KI} double CTD replacement mice.

(**a**) Similar LTP induced by one train of HFS in WT and GluA1^{C2KI}/GluA2^{C1KI} mice (WT = 117.54 ± 4.43%, n = 5 slices from 5 mice; A1^{C2KI}/A2^{C1KI} = 126.01 ± 6.85%, n = 5 slices from 5 mice; , t(8) = 1.037, p = 0.330). (**b**) Similar LTP induced by 4 trains of HFS (with 10 s inter-train intervals) in WT and GluA1^{C2KI}/GluA2^{C1KI} mice (WT = 160.69 ± 10.21%, n = 4 slices from 4 mice; A1^{C2KI}/A2^{C1KI} = 154.11 ± 15.00%, n = 5 slices from 5 mice; t(7) = 0.342, p = 0.742). (**c**) Similar LTD induced by LFS in field potential recordings in WT and GluA1^{C2KI}/GluA2^{C1KI} mice (WT = 76.44 ± 4.04%, n = 5 slices from 5 mice; A1^{C2KI}/A2^{C1KI} = 72.92 ± 5.03%, n = 6 slices from 6 mice; t(9) = 0.529, p = 0.609). (**d**) Similar LTD induced by LFS in whole cell recordings in WT and GluA1^{C2KI}/GluA2^{C1KI} mice (WT = 57.95 ± 5.49%, n = 5 slices from 5 mice; A1^{C2KI}/A2^{C1KI} = 56.90 ± 7.17%, n = 5 slices from 5 mice; t(8) = 0.116,

p = 0.901). Two tailed t-test at 95% confidence interval was used for all bar graphs. Scale bar: 0.25 mV/25 ms for Fig. 4a-c and 50 pA/25 ms for Fig. 4d.

Fig. 5. Impaired Glycine and NMDA Induced AMPAR Surface Delivery and Removal in GluA1^{C2KI} and GluA2^{C1KI} Cultured Neurons, Respectively.

(**a**,**b**,**c**) Sample images of WT (**a**), GluA1^{C2KI} (**b**) and GluA2^{C1KI} (**c**) cultured hippocampal neurons treated with ACSF (Ctrl), glycine (Gly) or glycine plus AP5 (AP5+Gly) and stained for synaptophysin and surface GluA2 (GluA2-NTD). (**d**) Summary graphs of normalized fluorescence intensities obtained from WT cultures (**a**) showing total surface GluA2 (Ctrl = 1.01 ± 0.04, n = 32 neurons; Gly = 1.31 ± 0.05, n = 31 neurons; ***p = 0.000005 compared to Ctrl; AP5+Gly = 1.09 ± 0.04, n = 30 neurons, p = 0.200 compared to Ctrl; $F_{(2,90)}$ = 12.673, p = 0.0000141) and synaptic GluA2 (Ctrl = 1.00 ± 0.09, n = 23 neurons; Gly = 1.40 ± 0.13, n = 20 neurons, **p = 0.010 compared to Ctrl; AP5+Gly = 0.95 ± 0.10, n = 18 neurons, p = 0.738 compared to Ctrl; $F_{(2,58)}$ = 5.080, p = 0.009). (**e**) Summary graphs of normalized fluorescence intensities obtained from GluA1^{C2KI} cultures (**b**) showing total surface GluA2 (Ctrl = 1.00 ± 0.04, n = 30 neurons; Gly = 1.01 ± 0.05, n = 31 neurons, p = 0.910 compared to Ctrl; AP5+Gly = 1.01 ± 0.05, n = 24 neurons, p = 0.861 compared to Ctrl; $F_{(2,82)}$ = 0.016, p = 0.984) and synaptic GluA2 (Ctrl = 1.00 ± 0.06, n = 20 neurons; Gly = 0.97 ± 0.09, n = 25 neurons, p = 0.813 compared to Ctrl; AP5+Gly = 0.85 ± 0.09, n = 19 neurons, p = 0.249 compared to Ctrl; $F_{(2,61)}$ = 0.768, p = 0.468). (**f**) Summary graphs of normalized fluorescence intensities obtained from GluA2^{C1KI} cultures (**c**) showing total surface GluA2 (Ctrl = 1.00 ± 0.046 n = 20 neurons; Gly = 1.45 ± 0.07, n = 19 neurons, ***p = 0.000004 compared to Ctrl; AP5+Gly = 1.09 ± 0.08, n = 16 neurons, p = 0.353 compared to Ctrl; $F_{(2,52)}$ = 14.634, p = 0.00006) and synaptic GluA2 (Ctrl = 1.00 ± 0.07, n = 16 neurons; Gly = 1.80 ± 0.15, n = 16 neurons, ***p = 0.00001 compared to Ctrl; AP5+Gly = 1.01 ± 0.12, n = 12 neurons, p = 0.945 compared to Ctrl;

$F_{(2,41)}$ = 15.767, p = 0.000083). (**g**,**h**,**i**) Sample images of cultured WT (**g**), GluA1^{C2KI} (**h**) and GluA2^{C1KI} (**i**) hippocampal neurons treated with ACSF (Ctrl), NMDA or NMDA plus AP5 (AP5+NMDA) and stained for surface GluA2 (GluA2-NTD) and synaptophysin. (**j**) Summary graphs of normalized fluorescence intensities obtained from WT (**g**) showing total surface GluA2 (Ctrl = 1.00 ± 0.04, n = 31 neurons; NMDA = 0.70 ± 0.05, n = 29 neurons; ***p = 0.000002 compared to Ctrl; AP5+NMDA = 0.92 ± 0.03, n = 11 neurons, p = 0.340 compared to Ctrl; $F_{(2,68)}$ = 13.920, p = 0.0000086) and synaptic GluA2 (Ctrl = 1.00 ± 0.07, n = 15 neurons; NMDA = 0.54 ± 0.05, n = 11 neurons, ***p = 0.00002 compared to Ctrl; AP5+NMDA = 0.86 ± 0.08, n = 10 neurons, p = 0.158 compared to Ctrl; $F_{(2,33)}$ = 12.210, p = 0.0001). (**k**) Summary graphs of normalized fluorescence intensities obtained from GluA1^{C2KI} (**h**) showing total surface GluA2 (Ctrl = 1.00 ± 0.07, n = 12 neurons; NMDA = 0.59 ± 0.09, n = 12 neurons, ***p = 0.001 compared to Ctrl; AP5+NMDA = 1.00 ± 0.01, n = 10 neurons, p = 0.992 compared to Ctrl; $F_{(2,31)}$ = 8.049, p = 0.002) and synaptic GluA2 (Ctrl = 1.00 ± 0.12, n = 11 neurons; NMDA = 0.47 ± 0.08, n = 12 neurons, **p = 0.001 compared to Ctrl; AP5+NMDA = 0.79 ± 0.12, n = 9 neurons, p = 0.179 compared to Ctrl; $F_{(2,29)}$ = 7.209, p = 0.003). (**l**) Summary graphs of normalized fluorescence intensities obtained from GluA2^{C1KI} (**i**) showing total surface GluA2 (Ctrl = 1.02 ± 0.06, n = 29 neurons; NMDA = 1.15 ± 0.07, n = 27 neurons, p = 0.176 compared to Ctrl; AP5+NMDA = 1.10 ± 0.13, n = 12 neurons, p = 0.541 compared to Ctrl; $F_{(2,63)}$ = 0.946, p = 0.394) and synaptic GluA2 (Ctrl = 1.00 ± 0.11, n = 13 neurons; NMDA = 0.87 ± 0.16, n = 10 neurons, p = 0.473 compared to Ctrl; AP5+NMDA = 0.93 ± 0.11, n = 12 neurons, p = 0.683 compared to Ctrl; $F_{(2,32)}$ = 0.268, p = 0.767). n represented number of neurons from 3 independent cultures from each genotype. One-way ANOVA followed by post-hoc Fisher's LSD multiple comparison test was used for Fig. 5d-f, j-i. Data were presented as mean ± SEM. **p < 0.01, ***p < 0.001. Scale bar: 20 μm.

Fig. 6. Impaired Glycine and NMDA Induced AMPAR Surface Delivery and Removal in GluA1^{C2KI} and GluA2^{C1KI} Hippocampal Slices, Respectively.

(**a,b,c)** Sample blots of surface protein biotinylation experiments showing surface GluA2 in acute hippocampal slices treated with glycine (Gly), NMDA (NMDA) or ACSF (Ctrl). (**d**) Summary graphs of normalized surface GluA2 in WT slices treated with Gly or NMDA compared to Ctrl (Gly: Ctrl = 1.00 ± 0.00, Gly = 1.45 ± 0.15, n = 4 slices from 3 independent experiments; $t_{(6)} = -2.954$, *p = 0.026; NMDA: Ctrl = 1.00 ± 0.00, NMDA = 0.62 ± 0.08, n = 8 slices from 3 independent experiments; $t_{(14)} = 4.537$, ***p = 0.0005). (**e**) Summary graphs of normalized surface GluA2 in GluA1^{C2KI} slices treated with Gly or NMDA compared to Ctrl (Gly: Ctrl = 1.00 ± 0.00, Gly = 1.06 ± 0.16, n = 6 slices from 3 independent experiments; $t_{(10)} = -0.356$, p = 0.729; NMDA: Ctrl = 1.00 ± 0.00, NMDA = 0.69 ± 0.13, n = 5 slices from 3 independent experiments; $t_{(8)} = 2.436$, *p = 0.041). (**f**) Summary graphs of normalized surface GluA2 in GluA2^{C1KI} slices treated with Gly or NMDA compared to Ctrl (Gly: Ctrl = 1.00 ± 0.00, Gly = 1.32 ± 0.09, n = 4 slices from 3 independent experiments; $t_{(6)} = -3.724$, **p = 0.010; NMDA: Ctrl = 1.00 ± 0.00, NMDA = 1.08 ± 0.17, n = 6 slices from 3 independent experiments; $t_{(10)} = -0.456$, p = 0.658). (**g**) Sample hippocampal section showing CA1 areas where immunofluorescence puncta were collected. (**h-j**) Sample images of a selected CA1 area showing surface GluA2 (green) and synaptophysin (red) in WT (**h**), GluA1^{C2KI} (**i**) and GluA2^{C1KI} (**j**) hippocampal sections. (**k-m**) Summary graphs of normalized total surface and synaptic GluA2 in WT (**k**) (Total surface GluA2: Ctrl = 1.00 ± 0.02, n = 17 slices from 3 independent experiments; NMDA = 0.68 ± 0.09, n = 11 slices from 3 independent experiments, ***p = 0.0003; Gly = 1.38 ± 0.09, n = 15 slices from 3 independent experiments, ***p = 0.0001; $F_{(2, 40)} = 23.704$, p = 0.0000002. Synaptic GluA2: Ctrl = 1.00 ± 0.06, n = 16 slices from 3 independent experiments; NMDA = 0.41 ± 0.07, n = 11 slices from 3 independent experiments, ***p < 0.000001; Gly = 2.03 ± 0.47, n = 11 slices from 3 independent experiments, *p =

0.016; $F_{(2, 35)}$ = 9.955, p = 0.0003), GluA1^{C2KI} (**l**) (Total surface GluA2: Ctrl = 1.00 ± 0.05, n = 13 slices from 3 independent experiments; NMDA = 0.78 ± 0.05, n = 12 slices from 3 independent experiments, **p = 0.008; Gly = 0.88 ± 0.04, n = 11 slices from 3 independent experiments, p = 0.103; $F_{(2, 33)}$ = 4.951, p = 0.013. Synaptic GluA2: Ctrl = 1.00 ± 0.09, n = 12 slices from 3 independent experiments; NMDA = 0.45 ± 0.15, n = 11 slices from 3 independent experiments, **p = 0.004; Gly = 0.91 ± 0.12, n = 8 slices from 3 independent experiments, p = 0.534; $F_{(2, 28)}$ = 6.159, p = 0.006) and GluA2^{C1KI} (**m**) (Total surface GluA2: Ctrl = 1.00 ± 0.03, n = 13 slices from 3 independent experiments; NMDA = 1.03 ± 0.12, n = 11 slices from 3 independent experiments, p = 0.790; Gly = 1.37 ± 0.10, n = 11 slices from 3 independent experiments, **p = 0.001; $F_{(2, 32)}$ = 5.301, p = 0.10. Synaptic GluA2: Ctrl = 1.00 ± 0.19, n = 13 slices from 3 independent experiments; NMDA = 1.04 ± 0.21, n = 11 slices from 3 independent experiments, p = 0.888; Gly = 3.71 ± 0.82, n = 10, **p = 0.002; $F_{(2, 31)}$ = 11.217, p = 0.000216) hippocampal sections. Two tailed t-test at 95% confidence interval was used for Fig. 6d-f and one-way ANOVA followed by two tailed t-test at 95% confidence interval for Fig.6k-m. Data were presented as mean ± SEM. *p < 0.05, **p < 0.01, ***p < 0.001. Scale bar: 200 μm for Fig. 6g and 10 μm for Fig. 6k-m. See **Supplementary Fig. S8** for full length Western blot scans.

Fig. 7. An increase in single channel conductance of AMPARs in WT and GluA2^{C1KI} following LTP induction.

(**a-c**) Sample LTP recordings for peak scaled non-stationary fluctuation analysis in WT (**a**, repeated 8 times with similar results), GluA1^{C2KI} (**b**, repeated 8 times with similar results) and GluA2^{C1KI} (**c,** repeated 7 time with similar results) mice showing absence of LTP in GluA1^{C2KI} mice. Scale bar: 25pA/30ms. (**d-f**) Representative EPSC traces and the conductance analysis in WT (**d**), GluA1^{C2KI} (**e**)

and GluA2^{C1KI} (**f**) mice before and after LTP induction (4 compressed trains of HFS, with 10 s inter-train intervals). Top: representative mean traces from baseline (light) and LTP (dark) superimposed with individual sweeps (grey). The carefully selected sweeps for analysis were aligned on the rise time phase, and scaled to the peak of their mean EPSC. Bottom: corresponding current-variance relationships (solid and dashed lines indicate a parabolic fit for baseline and LTP, respectively). Scale bars: 25pA/15ms. (**g**) Increased mean single channel conductance in WT and GluA2^{C1KI}, but not in GluA1^{C2KI} mice after LTP induction (WT: $\gamma_{baseline}$ = 9.82 ± 2.01 pS, γ_{LTP} = 13.41 ± 1.70 pS, n = 8 neurons from 8 mice, *p = 0.043; A1^{C2KI}: $\gamma_{baseline}$ = 9.38 ± 1.67 pS, γ_{LTP} = 9.83 ± 2.26 pS, n = 8 neurons from 8 mice, p = 0.791; A2^{C1KI}: $\gamma_{baseline}$ = 8.54 ± 1.75 pS, γ_{LTP} = 12.95 ± 1.47 pS, n = 7 neurons from 7 mice, **p = 0.009). (**h**) Rise time of EPSCs showing no changes after LTP induction in all genotypes (WT: baseline = 1.72 ± 0.11 ms, LTP = 1.80 ± 1.22 ms, n = 8 neurons from 8 mice, p = 0.986; A1^{C2KI}: baseline = 1.33 ± 0.07 ms, LTP = 1.31 ± 0.10 ms, n = 8 neurons from 8 mice, p = 0.900; A2^{C1KI}: baseline =1.88 ± 0.19 ms, LTP = 1.86 ± 0.21 ms, n = 7 neurons from 7 mice, p = 0.858). (**i**) Decay time of EPSCs showing no changes after LTP induction in all genotypes (WT: baseline = 9.12 ± 0.56 ms, LTP = 9.66 ± 0.71 ms, n = 8 neurons from 8 mice, p = 0.149; A1^{C2KI}: baseline = 8.29 ± 0.71 ms, LTP = 8.31 ± 0.58 ms, n = 8 neurons from 8 mice, p = 0.947; A2^{C1KI}: baseline =11.22 ± 0.88 ms, LTP = 10.81 ± 0.68 ms, n =7 neurons from 7 mice, p = 0.579). Paired t-test at 95% confidence interval was used for Fig. 7g-i. Data were presented as mean ± SEM. *p<0.05, **p<0.01.

Fig. 8. Spatial and contextual fear memory deficits in GluA1^{C2KI} and GluA2^{C1KI} mice.

(**a**) Learning acquisition of the hidden platform water maze test showing that GluA1^{C2KI} mice were slower to learn the location of the platform (between genotypes: WT: n = 11 mice, A1^{C2KI}: n = 9 mice, A2^{C1KI}: n = 11 mice; $F_{(2, 28)}$ = 7.318, **p = 0.003; day 5: WT = 40.79 ± 4.93s, A1^{C2KI} = 56.34 ± 2.89s,

$A2^{C1KI}$ = 48.11 ± 2.83s, $F_{(2, 28)}$ = 4.031, *p = 0.029; day 6: WT = 38.92 ± 4.70s, $A1^{C2KI}$ = 53.20 ± 4.00s, $A2^{C1KI}$ = 32.29 ± 5.56s, $F_{(2, 28)}$ = 4.447, *p = 0.021; day 7: WT = 29.36 ± 5.79s, $A1^{C2KI}$ = 54.39 ± 2.54s, $A2^{C1KI}$ = 35.29 ± 4.14s, $F_{(2, 28)}$ = 7,658, *p = 0.002). On last training day 8, all three genotypes reached the platform equally well (WT = 29.48 ± 5.98s, $A1^{C2KI}$ = 45.47 ± 5.03s, $A2^{C1KI}$ = 35.67 ± 4.29s, $F_{(2, 28)}$ = 2.292, p = 0.120). (**b**) Probe test at 2 h after the last training session showing that both WT and $GluA2^{C1KI}$ mice, but not $GluA1^{C2KI}$ mice, spent significantly more time (seconds) swimming in the target zone (WT: target = 20.591 ± 3.034, other = 9.185 ± 0.852, n = 11 mice, $t_{(10)}$ = 3.127, *p = 0.011; $A1^{C2KI}$: target = 8.94 ± 2.34, other = 8.07 ± 1.39, n = 9 mice, $t_{(8)}$ = 0.480, p = 0.644; $A2^{C1KI}$: target = 17.04 ± 2.21, other = 10.68 ± 0.88, n = 11 mice, $t_{(10)}$ = 2.392, *p = 0.039) compared other zones. (**c**) Probe test at 24 h after the last training session showing that both WT and $GluA2^{C1KI}$ mice, but not $GluA1^{C2KI}$ mice, spent significantly more time (seconds) swimming in the target zone (WT: target = 18.40 ± 2.64, other = 9.71 ± 1.14, n = 11 mice, $t_{(10)}$ = 2.588, *p = 0.025; $A1^{C2KI}$: target = 8.14 ± 1.24, other = 7.93 ± 1.31, n = 9 mice, $t_{(8)}$ = -0.113, p = 0.912; $A2^{C1KI}$: target = 14.08 ± 1.54, other = 10.34 ± 1.07, n = 11 mice, $t_{(10)}$ = 3.366, **p = 0.007) compared to other zones. (**d**) Learning acquisition of hidden platform water maze with enhanced training showing slower learning in $GluA1^{C2KI}$ mice (between genotypes: WT: n = 9 mice, $A1^{C2KI}$: n = 8 mice, $A2^{C1KI}$: n = 8 mice, $F_{(2, 22)}$ = 6.662, **p = 0.005; day 4: WT = 34.21 ± 3.17s, $A1^{C2KI}$ = 47.81 ± 3.96s, $A2^{C1KI}$ = 40.82 ± 3.98s, $F_{(2, 22)}$ = 3.464, *p = 0.049; day 5: WT = 30.92 ± 3.78s, $A1^{C2KI}$ = 46.63 ± 4.20s, $A2^{C1KI}$ = 35.33 ± 2.80s, $F_{(2, 22)}$ = 4.902, *p = 0.017; day 6: WT = 28.48 ± 6.72s, $A1^{C2KI}$ = 43.86 ± 7.94s, $A2^{C1KI}$ = 34.20 ± 7.55s, $F_{(2, 22)}$ = 1.118, p = 0.345; day 7: WT = 32.91 ± 6.86s, $A1^{C2KI}$ = 40.30 ± 7.32s, $A2^{C1KI}$ = 25.08 ± 6.72s, ($F_{(2, 22)}$ = 1.142, p = 0.337; day 8: WT = 21.09 ± 4.96s, $A1^{C2KI}$ = 36.63 ± 7.62s, $A2^{C1KI}$ = 24.31 ± 6.79s, ($F_{(2, 22)}$ = 1.611, p = 0.222; day 9: WT = 19.79 ± 5.01s, $A1^{C2KI}$ = 35.75 ± 6.93s, $A2^{C1KI}$ = 24.35 ± 7.77s, ($F_{(2, 22)}$ = 1.573, p = 0.230). (**e**) Probe test at 2 h after the last training session showing impaired memory in $GluA1^{C2KI}$ mice

(WT: target = 14.67 ± 1.43, other = 3.82 ± 0.38, n = 9 mice, $t_{(8)}$ = 8.69, ***p = 0.00002; $A1^{C2KI}$: target = 7.14 ± 1.39, other = 5.08 ± 0.79, n = 8 mice, $t_{(7)}$ = 1.480, p = 0.182; $A2^{C1KI}$: target = 17.51 ± 4.66, other = 3.06 ± 0.57, n = 8 mice, $t_{(7)}$ = 2.992, *p = 0.020). (**f**) Probe test at 24 h after the training showing impaired memory in $GluA1^{C2KI}$ mice (WT: target = 13.12 ± 1.45, other = 3.43 ± 0.38, n = 9 mice, $t_{(8)}$ = 7.804, ***p = 0.00005; $A1^{C2KI}$: target = 10.06 ± 3.44, other = 5.69 ± 0.93, n = 8 mice, $t_{(7)}$ = 1.274, p = 0.243; $A2^{C1KI}$: target = 17.60 ± 3.44, other = 3.55 ± 0.79, n = 8 mice, , $t_{(7)}$ = 3.488, *p = 0.010). (**g**) Freezing response (after the third foot shock) in response to three foot shocks in the conditioning chamber (WT: before = 2.55 ± 0.65%, after = 30.85 ± 4.29%, n = 12 mice, $t_{(11)}$ = -7.283, ***p = 0.00002; $A1^{C2KI}$: before = 2.18 ± 0.63%, after = 29.31 ± 4.38%, n = 12 mice, $t_{(11)}$ = -6.788, ***p = 0.00003; $A2^{C1KI}$: before = 5.61 ± 1.42%, after = 40.62 ± 3.21%, n = 12 mice, $t_{(11)}$ = -10.470, ***p = 0.0000005). (**h**) Contextual memory test at 2 h after conditioning (WT = 38.16 ± 5.57%, n = 12 mice; $A1^{C2KI}$ = 41.55 ± 5.92%, n = 12 mice, p = 0.681 compared to WT; $A2^{C1KI}$ = 20.43 ± 3.32%, n = 12, *p = 0.012 compared to WT; $F_{(2, 33)}$ = 5.004, p = 0.013). (**i**) Contextual memory test at 24 h after conditioning (WT = 35.47 ± 5.87%, n = 12 mice; $A1^{C2KI}$ = 43.03 ± 8.47%, n = 12 mice, p = 0.47 compared to WT; $A2^{C1KI}$ = 21.61 ± 2.49%, n = 12 mice, *p = 0.041 compared to WT; $F_{(2,33)}$ = 5.00, p = 0.013). (**j**) Freezing response (after the second foot shock) in response to two foot shocks in the conditioning chamber (WT: before = 3.59 ± 1.23%, after = 35.66 ± 7.33%, n = 9 mice, **p = 0.002; $A1^{C2KI}$: before = 1.52 ± 0.33%, after = 32.63 ± 6.89%, n = 8 mice, **p = 0.003; $A2^{C1KI}$: before = 5.48 ± 1.31%, after = 42.96 ± 7.46%, n = 9 mice, ***p = 0.001). (**k**) Contextual memory test at 2 h after conditioning (WT = 33.00 ± 6.197%, n = 9 mice; $A1^{C2KI}$ = 18.62 ± 3.67%, n = 8 mice, *p = 0.040 compared to WT; $A2^{C1KI}$ = 20.04 ± 3.19%, n = 9 mice, *p = 0.055 compared to WT; $F_{(2, 23)}$ = 2.982, p = 0.071). (**l**) Contextual memory test at 24 h after conditioning (WT = 33.29 ± 5.75%, n = 9 mice; $A1^{C2KI}$ = 30.41 ± 6.79%, n = 8 mice, p = 0.746 compared to WT; $A2^{C1KI}$ = 18.72 ± 3.57%, n = 9 mice, *p =

0.047 compared to WT; $F_{(2, 23)} = 2.077$, p = 0.148). (**m**) Contextual memory test on the third day following pre-exposure to the conditioning chamber without foot shocks on day 1 and two foot shocks on day 2 (WT = 32.21 ± 4.31%, n = 17 mice; $A1^{C2KI}$ = 32.86 ± 4.68%, n = 14 mice, p = 0.920 compared to WT; $A2^{C1KI}$ = 20.17 ± 2.79%, n = 17 mice, *p = 0.025 compared to WT; $F_{(2, 45)} = 3.372$, p = 0.043). Paired t-test at 95% confidence interval was used for Fig. 8b,c,e,f,g, one-way ANOVA followed by post-hoc Fisher's LSD multiple comparison test for Fig. 8h,i,k, one-way ANOVA followed by two tailed t-test at 95% confidence interval for Fig. 8l,m. Data were presented as mean ± SEM. *p<0.05, **p<0.01,***p<0.001.

Methods:

Generation of GluA1^{C2KI} mice

The GluA1^{C2KI} mouse model, where the C-terminal domain (CTD) of GluA1 (EFCYKSRSESKRMKGFCLIPQQSINEAIRTSTLPRNSGAGASGGSGSGENGRVVSQDFPKSMQSIPCMSHSSGMPLGATGL) is replaced by the CTD of GluA2 (EFCYKSRAEAKRMKVAKNAQNINPSSSQNSQNFATYKEGYNVYGIESVKI), was generated by using standard homologous recombination techniques in embryonic stem (ES) cells as described previously (Fig. S1 and S2, *ref 19,21,49*) in collaboration with Biocytogen (Worcester, MA, USA). Briefly, a targeting vector was constructed (by using a BAC clone, Rp23-118D11, Invitrogen, isolated from a C57BL/6J mouse genomic library) in such a way that the C-terminus of GluA1 (81 AA) was replaced with the C-terminus of GluA2 (50 AA) using an overlap extension-PCR method. The targeting vector contained a Frt-flanked Neo resistance positive selection marker inserted 315bp upstream of exon15, a number of new restrictions sites (i.e. EcoRI and VspI) used for diagnostic restriction

digestions to confirm the homologous recombination events and two homology arms (left: 4.6 kb; right: 4.7 kb). A DTA negative selection marker was inserted downstream of the right arm. The vector was verified by sequencing the entire construct. After linearization, the targeting vector was transfected into C57BL/6J-derived ES cells (Biocytogen Worcester, MA, USA) by electroporation (BTX, USA). Positive ES clones were identified first by long-range PCR screening methods (forward primer 1: ctgtgaacctggttcaagatcacac; reverse primer 1: cagaggccacttgtgtagcg; forward primer 2: gctcgactagagcttgcgga; reverse primer 2: gccttgctgatcataccttagcatc) and then confirmed by Southern blotting analysis with both 5'and 3'probes. The 5' and 3' probes were obtained by PCR amplification from the C57BL/6J genomic DNA using following primers. 5' probe (451bp) forward: gagcataggagaacagtgtcag, 5' probe reverse: actggatgtctaattggactatgc; 3' probe (412bp) forward: cacactgatgggcatgtcatc; 3' probe reverse: ctgtgacttccactagcagg. The confirmed ES clones were injected into Balb/c blastocysts and implanted into pseudopregnant females. 10 chimeric male mice were crossed with C57BL/6J females to obtain F1 mice carrying the recombinant allele containing the C-terminus of GluA2 (50 AA) and Neo selection marker. The resulting pups were bred for germline transmission of the recombination event by using PCR strategy. Heterozygous males were then mated with the FLIP females to remove the Neo marker. The FLIP mice have a pure C57BL/6J background (Jackson Laboratories). Homozygous mutant mice were obtained by inter-crossing heterozygous littermates. Because the ES cell line that we used for creating the GluA1^{C2KI} mice was derived from the C57BL/6J mice, therefore, all the mice used for this study were of a pure C57BL/6J genetic background, eliminating a potential effect of variable genetic backgrounds on the phenotype of the mice. The PCR primers used for mouse tail DNA genotyping included: WT forward: cagcaataccatcaatgaagaccatacg; WT reverse: gctgaattgccctccatatggttg; GluA1^{C2KI} forward: gagttctgttacaagtcaagggcc (or ctttgtttttggcactgaagggc); GluA1^{C2KI} reverse: gctgaattgccctccatatggttg; Frt forward:

gagacatgcacaatgatggaggc; Frt reverse: cttctctgggacaggagataccac. All the GluA1^{C2KI} mice used in this study were homozygous mice for the CTD replacement and their wild type littermate offspring from the heterozygous breeders.

Generation of GluA2^{C1KI} mice

The GluA2^{C1KI} mouse model, where the CTD of GluA2 (EFCYKSRAEAKRMKVAKNAQNINPSSSQNSQNFATYKEGYNVYGIESVKI) is replaced by the CTD of GluA1 (EFCYKSRSESKRMKGFCLIPQQSINEAIRTSTLPRNSGAGASGGSGSGENGRVVSQDFPK SMQSIPCMSHSSGMPLGATGL), was generated by using standard homologous recombination techniques in embryonic stem (ES) cells as described previously (Fig. S1 and S2, *ref 19,21,49*, in collaboration with Biocytogen (Worcester, MA, USA). Briefly, a targeting vector was constructed (by using a BAC clone, RP23-409L22; Invitrogen, isolated from a C57BL/6J mouse genomic library) in such a way that the C-terminus of GluA2 (50 AA) was replaced with the C-terminus of GluA2 (81 AA) using an overlap extension-PCR method. The targeting vector contained a Frt-flanked Neo resistance positive selection marker inserted 371bp upstream of exon15, a number of new restriction sites (i.e. XbaI and DraIII) used for diagnostic restriction digestions to confirm the homologous recombination events and two homology arms (left: 4.6 kb; right: 5.3 kb). A DTA negative selection marker was inserted downstream of the right arm. The vector was verified by sequencing the entire construct. After linearization, the targeting vector was transfected into C57BL/6J-derived ES cells (Biocytogen, Worcester, MA, USA) by electroporation (BTX, USA). Positive ES clones were identified first by long-range PCR screening methods (forward primer: gctcgactagagcttgcgga; reverse primer: actccctcccaagagtttaatccac) and then confirmed by Southern blotting analysis with both 5'and 3'probes.

The 5’ and 3’ probes were obtained by PCR amplification from the C57BL/6J genomic DNA using following primers. 5’ probe (364bp) forward: gaggtagcagacacacagac, 5’ probe reverse: gtggattgtctttgtgaaag; 3’ probe (337bp) forward: agtcttatctttgcccatcagg; 3’ probe reverse: aagctagagagctggacttga. The confirmed positive ES clones were injected into Balb/c blastocysts and implanted into pseudopregnant females. 5 chimeric male mice were crossed with C57BL/6J females to obtain F1 mice carrying the recombinant allele containing the C-terminus of GluA1 (81 AA) and Neo selection cassette. The resulting pups were bred for germline transmission of the recombination event by using the PCR strategy. Heterozygous males were then mated with the FLIP females to remove the Neo cassette. The FLIP mice have pure a C57BL/6J background (Jackson Laboratories). Homozygous mutant mice were obtained by inter-crossing heterozygous littermates. Because the ES cell line that we used for creating the GluA2^{C1KI} mice was derived from the C57BL/6J mice, therefore, all the mice used for this study were of a pure C57BL/6J genetic background, eliminating a potential effect of variable genetic backgrounds on the phenotype of the mice. The PCR primers used for mouse tail DNA genotyping included: WT forward: gttacaagtcaagggccgagg; WT reverse: gcaggttagtcactggtcagg; GluA2^{C1KI} forward: ccctgcatgagccacagttc; GluA2^{C1KI} reverse: gcaggttagtcactggtcagg; Frt forward: actgacactctgtcttaggaatct; Frt reverse: agctgaagaaatttggtggactc. All the GluA2^{C1KI} mice used in this study were homozygous mice for the CTD knock-in replacement and their wild type littermate offspring derived from the heterozygous breeders.

Generation of GluA1^{C2KI}/GluA2^{C1KI} CTD double replacement mice

To produce GluA1^{C2KI}/GluA2^{C1KI} mice (homozygous for both CTD replacements, i.e. the CTD of GluA1 is replaced by that of GluA2 and the CTD of GluA2 is replaced by that of GluA1), the GluA1^{C2KI} was first bred with GluA2^{C1KI} to obtain heterozygous mice for both CTD replacements, which were

subsequently intercrossed to produce homozygous GluA1^{C2KI}/GluA2^{C1KI} mice (Fig. S1 and S2).

Housing, maintenance and use of the mice

Mice were group housed (2-5 mice per cage) on a 12h/12h light/dark cycle with food and water ad libitum. All experimental procedures were conducted in accordance with the guidelines of the Canadian Council on Animal Care (CCAC) and approved by the Animal Care Committee at the Hospital for Sick Children, Canada and Southeast University, China. All experiments were performed blind to the genotype of the mice, that is, the mice were coded by an independent investigator before the experimentation and decoded after the completion of the experiments for data grouping and analyses. All the data collection, animal assignment, drug treatment and experimental conditions were randomized with regard to the genotypes of the mice.

Antibodies, chemicals and other reagents

Primary and secondary antibodies include: Rabbit polyclonal anti-GluA1-CTD (Millipore, Cat#MAB2263), Rabbit polyclonal anti-GluA1-NTD (Cell signaling technology, Cat#T8850), Mouse monoclonal anti-GluA2-NTD (Millipore,Cat#MAB397), Rabbit polyclonal anti-GluA3 (Cell signaling technology, Cat#4676), Rabbit polyclonal anti-GluA4 (Cell signaling technology, Cat#T8030), Rabbit polyclonal anti-p-GluA1-831 (Santa Cruz, Cat#sc-16313), Rabbit polyclonal anti-p-GluA1-845 (Cell signaling technology, Cat#8084), Rabbit polyclonal anti-p-GluA2-Tyr (869/873/876) (Cell signaling technology, Cat#3921). Mouse monoclonal anti-MAP2 (Millipore, Cat#MAB3418), Rabbit polyclonal anti-NR1 (Millipore, Cat#AB9864), Rabbit polyclonal anti-NSF (Cell signaling technology, Cat#3924), Rabbit polyclonal anti-Pan-cadherin (Cell signaling technology, Cat#4068), Mouse monoclonal anti-PSD95 (Millipore, Cat#MABN68), Rabbit polyclonal anti-SAP97 (Abcam, Cat#ab134156), Rabbit polyclonal anti-Synapsin1 (Bioworld, Cat#BS4116), Rabbit polyclonal anti-Synaptophysin (Cell

signaling technology, Cat#D35E4), Mouse monoclonal anti-Tubulin (Sigma-Aldrich, Cat#T9026), Goat anti-rabbit (Genscript, Cat#A00098), Goat anti-mouse (Genscript, Cat#A00160), Alexa Fluor 488 donkey anti-mouse IgG (Thermo-Fisher, Cat#R37114), Alexa Fluor 555 goat anti-mouse IgG (Thermo-Fisher, Cat#A-21422), Alexa Fluor 555 donkey anti-rabbit IgG (Thermo-Fisher, Cat#A-31570), Alexa Fluor 633 goat anti-mouse IgG (Thermo-Fisher, Cat#A-21050). Drugs include: Picrotoxin (Sigma-Aldrich, Cat#R284556), (RS)-3,5-DHPG (Tocris, Cat#0342), MPEP (Tocris, Cat#1212), D-AP5 (Tocris, Cat#0106), Spermine (Sigma-Aldrich, Cat#55513), Tetrodotoxin (Sigma-Aldrich, Cat#A3109), Cyclothiazide (Tocris, Cat#0713), Neurobasal A (Thermo-Fisher, Cat#10888022), B27 (Thermo-Fisher, Cat#17504044), NMDA (Tocris, Cat#0114), NBQX (Sigma-Aldrich, Cat#N183), Biotin-XX, SSE (Thermo-Fisher, Cat#B6352), Rhodamine phalloidin (Thermo-Fisher, Cat#R415) DAPI (Cayman Chemical, Cat#28718-90-3), Poly-D-lysine (Sigma-Aldrich, Cat#P7280), GlutaMax (Thermo-Fisher, Cat#35050061), Diamond Antifade Mountant (Thermo-Fisher, Cat#P36965). Streptavidin Trial Kit was purchased from Thermo-Fisher (Cat#65801D).

Slice electrophysiology

All the electrophysiological recordings were conducted at the Schaffer collateral - commissural pathway in the hippocampus as previously described[19,21,49,50]. Briefly, the mouse brains were quickly removed and sagittal 360 μm hippocampal slices prepared in ice-cold artificial cerebrospinal fluid (ACSF) saturated with 95% O_2/5% CO_2. ACSF contained (in mM): 120.0 NaCl, 3.0 KCl, 1.2 $MgSO_4$, 1.0 NaH_2PO_4, 26.0 $NaHCO_3$, 2.0 $CaCl_2$, and 11.0 D-glucose. The slices were recovered at 28 ºC for at least 2 hrs before a single slice was transferred to a submersion chamber perfused with 95% O_2 / 5% CO_2 saturated ACSF with (for whole-cell recordings) or without (for field recordings) 100 μM picrotoxin. Perfusion flow rate was kept constant at 2 ml/min. Hippocampal CA1 neurons were visualized using an

infrared differential interference contrast microscope (Zeiss Axioscope or Olympus X51). Synaptic response was evoked at 0.067 Hz for field potentials and 0.1 Hz for whole-cell currents, and recorded with glass pipettes (3-4 MΩ) filled with either ACSF (for field) or the intracellular solution (for whole-cell) containing (in mM) 130.0 $CsMeSO_4$, 5.0 NaCl, 1 $MgCl_2$, 0.05 EGTA, 10.0 HEPES, 3.0 Mg-ATP, 0.3 Na_3GTP, and 5.0 QX-314 (pH 7.5) (280-300 mOsm). For field recordings, low-frequency stimulation (LFS, 900 pulses at 1 Hz) and paired-pulse (interval at 50 ms) low-frequency stimulation (PP-LFS, 900 paired pulses at 1 Hz) were used to induce NMDAR- and mGluR-LTD, respectively. LTP was induced by 1 or 4 trains of high-frequency stimulation (HFS, 100 Hz, 1 s) with an inter-train interval of 10 s or 5 min. For input-output experiments, the stimulus intensity was increased gradually from 0.1 mA, 0.2 mA, 0.3 mA to 0.4 mA. Paired-pulse facilitations were obtained at inter-pulse intervals of 25 ms, 50 ms, 100 ms, 200 ms, 500 ms or 1 s, and calculated as the ratios of the second response peak values over the first response peak values. For LTD whole-cell experiments, cells were clamped at -65 mV throughout the recording except during LTD induction (LFS: 900 pulses at 5 Hz, at -40 mV holding potential; PP-LFS: 600 paired pulses at1 Hz, at -65 mV holding potential). DHPG-LTD was induced by bath application of 100 μM (RS)-3,5-DHPG for 10 mins. The age of mice was 13-15 days for LFS-LTD and non-SFA experiments and 3-4 weeks for PP-LFS-LTD, DHPG-LTD and all other LTP experiments. LTP and LTD were calculated and statistically evaluated by comparing the mean values of the last 10 min of the recording and the mean values of the entire baseline. For current/voltage (I/V) relationship and rectification index experiments, synaptic currents (5 responses at each holding potential) mediated by NMDARs ($EPSC_{NMDAR}$) or AMPARs ($EPSC_{AMPAR}$) were obtained for the following holding potentials (-80 mV, -60 mV, -40 mV, -20 mV, 0 mV, 20 mV, 40 mV, 60 mV), with 100 μM spermine and 50 μM D-AP5 (for $EPSC_{AMPAR}$) or 10 μM NBQX (for $EPSC_{NMDAR}$) added to the extracellular solution, respectively. The responses were normalized to those obtained at -80 mV.

The rectification index of $EPSC_{AMPAR}$ was calculated by the ratio of the slopes of the line connecting 0 to 60 mV and -60 to 0 mV. For $EPSC_{NMDAR}/EPSC_{AMPAR}$ ratio experiments, $EPSC_{AMPAR}$ was the peak value obtained at -70 mV, whereas $EPSC_{NMDAR}$ was the response amplitude at +40 mV taken 40 ms after the onset of the response. For miniature EPSCs (mEPSCs), the responses were recorded at -70 mV in the presence of the 100 μM picrotoxin and 1 μM TTX. In all of the whole-cell recordings, cell series resistance was monitored throughout experiments by applying a -3 mV step at the end of each response sweep and the experiment was excluded from analysis if the resistance changed by more than 20%. For the outside-out patch experiments, after the whole-cell patch clamp mode was obtained from the CA1 neuron at -70 mV, the patch pipette (4-7 MΩ) was slowly pulled away from the soma until a high-resistance seal was reformed. AMPAR-mediated currents of the patch were evoked by a fast puff delivered from a pipette (3-5 MΩ) filled with ACSF containing 100 μM picrotoxin, 50 μM D-AP5, 100 μM cyclothiazide, 1 μM TTX and 1 mM L-glutamate acid monosodium salt monohydrate using the PV830 Pneumatic Picopump (WPI). All recording data acquisition and analysis were done using the pCLAMP 10.2 (Axon Instruments) and MiniAnalysis program (Synaptosoft). n in all recording figures represents the number of slices/neurons and at most two slices/neurons from each animal were used.

Peak-scaled, non-stationary fluctuation analysis

The single channel conductance (γ) of synaptic AMPARs in WT and mutant mice was estimated using peak-scaled non-stationary fluctuation analysis (ps-NSFA) as described previously[34]. Neurons were clamped at -70 mV and whole-cell EPSCs were strictly selected using WinLTP and Mini Analysis software based on the following criteria: (1) precise alignment of responses on the rising phase of EPSCs; (2) no contamination by spontaneous or polysynaptic currents; and (3) complete decay from the peak EPSCs. The variance of fluctuation of the decay was analyzed and plotted against the mean

amplitude of EPSCs. The single channel conductance was calculated by fitting the plot to a second polynomial equation, $\sigma^2 = iI - I^2/N + b_1$, where σ^2 is the variance, I is the mean current, N is the number of channels activated, i is the single channel current and b_1 is the background noise. For the conductance conversion (i.e. $\gamma = i/V$), the driving force (V) was set to -70 mV. LTP was induced by HFS (100 Hz, 1 s delivered 4 trains with an inter-train interval of 10 s) in current-clamp mode. The kinetics of EPSCs were calculated by measuring the 20-80% rise time (τ_{rise}) and 62% decay time (τ_{decay}), respectively, using the Clampfit.

Immunohistochemistry of brain sections

The procedures for brain processing and immunohistochemistry were described previously[21,49]. Briefly, mice were anesthetized by 10% chloral hydrate and subjected to cardiac perfusion with 0.1 M phosphate-buffered saline (PBS) followed by 4% paraformaldehyde (PFA in PBS). The brain was then dissected and further fixed in 4% PFA for an additional 24 h, and then transferred to 30% sucrose in PBS solution till it was saturated. The brain was embedded in Tissue-Tek® O.C.T. compound, frozen in liquid nitrogen and stored at - 80 °C, before being sliced to 25 μm coronal crystat sections at -20 °C (Leica CM1950). The brain sections were transferred to a glass slide coated with poly-D-lysine for immunostaining. Sections were washed with PBS, permeabilized by 0.1% Triton X-100 in PBS for 2 h, blocked with 10% fetal bovine serum for 1 h, and incubated with primary antibodies overnight at 4°C, and then appropriate secondary and DAPI at 37 °C for 2 h. Following washing, the stained coverslips were mounted using the ProLong Diamond Antifade mounting medium for image collections.

Neuronal culture, treatment and immunostaining

Hippocampal neuronal cultures were prepared from postnatal day 1 (P1) pups as previously described[49,50] with minor modifications. Briefly, hippocampal CA1 regions were dissected in ice-cold

0.1 M PBS, tissues were trypsinized (0.25%) at 37 ºC for 15 min, dissociated by trituration, and plated onto poly-D-lysine (50 μg/ml) coated glass coverslips (60,000 cells/ml). The cultures were maintained by replacing half of the medium with fresh medium every 3-4 days. The maintenance medium contained Neurobasal A, 0.5 mM GlutaMax and B27. At 17-18 DIV, neurons were either treated with D-AP5 (50 μM) or fresh neurobasal medium for 10 min, then with NMDA (25 μM) or glycine (200 μM) for 3 min, to trigger AMPAR endocytosis or surface delivery. Following the treatment, neurons were washed with PBS and incubated at 37 ºC in fresh conditional medium for additional 10 min. The cells were then fixed with ice-cold 4% paraformaldehyde and 4% sucrose for 30 min. For surface GluA2 staining, the fixed cells were blocked with 5% FBS in 0.1M PBS for 1 h and incubated with GluA2-NTD antibody overnight at 4ºC. The cells were then permeabilized with 0.25% TritonX-100 for 30 min, blocked again with 5% FBS in 0.1M PBS again for 1 h, and incubated with either GluA2 or synaptophysin antibody for at least 8 h at 4 ºC. For permeabilized (total protein) staining, the fixed cells were immediately treated with 0.25% TritonX-100 for 30 min before being blocked with 5% FBS in 0.1M PBS for 1 h and incubation with primary antibodies overnight at 4 ºC. After the primary antibody incubation, cells were incubated with rhodamine-conjugated phalloidin or appropriate secondary antibodies for 1 h at room temperature. After washing with 0.1M PBS, coverslips were mounted using the ProLong Diamond Antifade mounting medium for image collection.

Microscope setups, image collection and analysis

For spine analyses, confocal images were obtained at room temperature using a Zeiss LSM 700 at 2048 ×2048 pixels using Zeiss 63× (NA 1.4, oil immersion) objective with the same settings and configurations for all samples within each experiment. Spines were defined as any dendritic protrusions of 0.3-4 μm in length. For analyses of synaptic proteins, the fluorescence puncta (with an area of greater than 0.1 μm^2) were automatically selected and counted and manually verified. For each

treatment, approximately 10-25 neurons from at least 3 independent cultures and a total of 100-150 μm linear dendrites per neuron were randomly selected, measured and averaged. For immunohistochemistry staining, confocal images were obtained at room temperature on Zeiss LSM 700 at 2048 ×2048 pixels using Zeiss 5× (NA 0.15, dry) objective with the same settings and configurations for all samples within each experiment. The fluorescence puncta from CA1 apical dendritic areas were selected and counted and manually verified. All images were initially acquired through the Zen 2010 software (Zeiss). AimImageBrowser (Zeiss) software was used to adjust the image brightness/contrast and to extract a sub-region. All measurements were performed using the ImageJ (NIH) software.

Western blot analysis and immunoprecipitation

Whole brain protein lysates were prepared from 3 to 5 week-old mutant and their WT control littermates as previously described[50]. One mouse brain was homogenized in a Dounce homogenizer with 1.5 ml ice-cold lysis buffer containing (in mM): 20 Tris-HCl (pH 7.5), 150 NaCl, 1 EDTA, 1 EGTA, 1% Triton X-100, 2.5 sodium pyrophosphate, 1 β-glycerophosphate, 1 Na3VO4, 20 NaF, and 1% protease inhibitor cocktail and phosphatase inhibitor (Roach) and kept at 4 ℃ for 40 min before debris was removed by centrifugation at 14,000g for 10 min. The protein samples were either stored or mixed with 25% volume of 5×SDS loading buffer (250 mM Tris-HCl, 10% SDS, 0.5% bromophenol blue, 50% glycerol, 5% beta-mercaptoethanol, pH 7.4) for electrophoresis on a SDS-PAGE ployacrylamide gel and electrotransfered to a PVDF filter. The filter was then blocked with 5% dry milk in TBST (20 mM Tris-HCl, 9% NaCl, 1% Tween-20, pH 7.6) and incubated overnight at 4 ℃ with suitable primary antibodies in TBST. Following washing and incubation with appropriate secondary antibodies, the filter was washed extensively and developed using an enhanced chemiluminescence (Thermo) method of detection and analyzed using the AlphaEaseFC software as per manufacturer's instruction. The amount of total

protein loaded was controlled by normalizing each tested protein with anti-tubulin immunoreactivity on the same blot. For the biotinylation experiments of acute slices, protein loading and surface biotin labeling efficiency were further controlled by normalizing the protein of interest (i.e. surface GluA2) with the anti-Pan-Cadherin immunoreactivity on the same blot. For immunoprecipitation experiments, 300 µl of the protein lysate (200–300 µg, normally pooled from 1/5 to 1/4 whole brain lysate) was incubated with GluA1-NTD or GluA2-NTD antibodies at 4°C with constant gentle rocking over night, followed by addition of 30 µl of Protein A/G agarose beads slurry (Santa Cruz Biotechnology, Inc.) and further incubation for 4 h at 4°C. The beads were carefully harvested and washed thoroughly with the lysis buffer five times and resuspended in loading buffer for Western blot analysis.

Biotinylation and immunofluorescence assays of surface AMPARs in hippocampal slices

Brain slices were prepared according to the same procedure as for electrophysiological recordings. Slices were recovered at room temperature in ACSF saturated with 95% O2 /5% CO2 for 3-4 hours. Then slices were then transferred to a treatment chamber containing the same 95% O2 /5% CO2 saturated ACSF and treated with NMDA (25 µM), glycine (200 µM) or ACSF alone for 3 min at room temperature. For biotinylation assay, after 10 min recovery in the saturated ACSF, slices were transferred to a labeling chamber and incubated with 1 mM Biotin-XX, SSE (B6352, Thermo) in ACSF at 4 ℃. 30 min later, the slices were quenched three times with 20 mM Tris-HCl (pH 7.35) at 4 ℃ for 10 min. After the labeling, slices were rapidly placed into ice-cold lysis buffer, and lysed for 45 minutes. Debris were removed by centrifugation at 14,000 g in 4 ℃ for 10 min. Each (400 µl) of the biotin-labeled supernatant samples was incubated with 50 µl of lysis buffer prewashed streptavidin-coated magnetic bead slurry (65801D, Thermo) overnight at 4℃ with gentle rotation. The beads were washed with ice-cold lysis buffer for 5 times before being resuspended in 40 µl 2×SDS buffer (100 mM

Tris-HCl, 4% SDS, 0.2% bromophenol blue, 20% glycerol, 2% beta-mercaptoethanol, pH 7.4). Samples were separated on SDS-PAGE polyacrylamide gel for western blot analysis. For immunofluorescence staining, after 20 min recovery in the saturated ACSF, slices were fixed in 4% PFA for 4 h, and then transferred to 30% sucrose in PBS solution till it was saturated. Then the slices was embedded in Tissue-Tek® O.C.T. compound, frozen in liquid nitrogen and stored at - 80 °C, before being sliced to 25 μm coronal crystat sections at -20 °C (Leica CM1950).

Behavioral tests

Previously described procedures for animal handling and testing[29,49] were followed with some modifications as detailed below.

Subjects. Animals were tested at the age of 3 ± 0.5 months. The CTD replacement mutant and their WT littermate control groups were sex-balanced and handled daily for three days before the following experiments. All the behavioral tests were performed during the light cycle. The mice were tested in open field, then elevated plus maze and finally water maze, with one week interval between these tests. Separate groups of mice were used for the fear memory test.

Open field test. The open field apparatus is a rectangular plexiglass box (35×35×35 cm) comprising of four walls and an open roof. The illumination in the room was provided by centrally placed in-ceiling dim lights. All mice were individually tested in one 5 min session. Each subject was introduced to the apparatus in the same place of the arena near the center and allowed to explore the maze for 5 min. The apparatus was cleaned thoroughly with 75 % ethanol before each subject was tested. The movement of the mouse was video tracked and analyzed off-line using ANY-maze software (USA). The box was divided into central (center 15 cm diameter) and peripheral fields for analysis.

Elevated plus maze test. The elevated plus maze was made of two open arms (30×5 cm) without any walls and two enclosed arms (30x5 cm) with 15 cm high walls on each side. These arms were elevated 60 cm above the ground. Again all mice were individually tested in one 5 min session. The mouse was placed in the center of the maze and allowed to explore for 5 min. The maze was cleaned thoroughly with 75 % ethanol before each mouse was tested. Traces of movement were tracked and analyzed off-line using ANY-maze software (USA).

Water maze test. The water maze consisted of a circular pool (120 cm diameter) filled with water (22 ± 2°C). The water was made opaque with non-toxic white chalk. The platform (10 cm wide) was located approximately 1 cm below the water level. On the first 3 days, the mice were trained to locate a visible platform (indicated with a visible red flag). Each subject was given four trials (with 1.5 h inter-train interval) per day. Each trial began by placing the mouse in the water, near and facing the wall of the pool. The starting points for each subject were chosen randomly from any of the three quadrants other than the one with the platform. Each subject was allowed 60 s to find the platform and if it failed to reach the platform within 60 s, it was guided by the experimenter to the platform and allowed to stay on the platform for 10 s. The mice that did not reach the platform during a trial were assigned a latency of 60 s. Upon removal from the maze, the mice were dried with absorbent papers, placed on a warm platform and returned to their home cages. After the visible platform test was completed, the mice were then trained for the next eight or nine days to locate a hidden platform with three or four training trials per day (with 3-4 h inter train interval). Short-term or long-term memory tests were conducted by probe trials (platform removed) 2 h or 24 h after the last trial on the last day of the hidden platform training. The entire travel of the mouse was tracked and analyzed off-line with ANY-maze software. The time that the mouse spent in the target quadrant or target zone (30 cm diameter around the platform) during

the probe trial was used as a measure of spatial memory retention. Mice with more than 20 s of floating during learning acquisition were excluded from analysis.

Contextual and cued conditioned fear. The conditioning chamber contained one foot-shock box (30 × 26 × 30 cm) with a speaker and a light (Freeze Frame, USA). The floor of the box consisted of stainless steel bars that were connected to a computer, which controlled the duration of a test session, timing, and intensity and duration of the shock or sound. Background noise was 55 dB. The subject mouse was allowed to explore the chamber for 300 s before the onset of a discrete conditioned stimulus (CS), which consisted of continuous sound (2000 Hz, 80 dB) lasting 40 s. During the last 2 s of this CS period a subject was exposed to an unconditioned stimulus (US), a continuous foot shock (0.7 mA). This CS-US training paradigm was repeated two or three times with an inter-train interval of 40 s. 10 s later, mice were removed from the chamber and returned to their home cages. Approximately 2 h or 24 h later, subjects were given a 3 min contextual conditioning test in the same chamber where they were trained. The cued test (7 min) was performed 2 h after the contextual test. For the cued test the chamber was completely altered by covering the floor and walls with gray paperboard. During the first 5 min of the test the CS was not presented (pre-CS stage), after which subjects were exposed to the same tone given during the training but without any foot shocks. In the context pre-exposure version of the fear conditioning paradigm, each mouse was allowed to explore the conditioning chamber for 4 min without any foot shocks or tone. On the following day, the mouse was placed back to the chamber and immediately given two foot shocks (0.7 mA, each lasting 2 s with a 1 s interval). The mouse was removed from the chamber right after the shocks. 24 h later the mouse was tested for 3 min for a freezing response in the conditioning chamber. The chamber was cleaned with 10% alcohol after each subject was trained or tested. Behavior of the mice was recorded and analyzed off-line using automated motion detection software Freeze Frame (USA).

Statistical Methods

All the averaged data in the graphs were stated as mean ± SEM and statistically evaluated by Student's *t*-test for comparisons of two groups, or ANOVA (one-way, two-way or repeated measures wherever appropriate) for comparisons of more than two groups followed by post-hoc Fisher's LSD multiple comparison test using the SPSS program. $p < 0.05$ was considered as significant (*$p < 0.05$, **$p < 0.01$, ***$p < 0.001$). The variances within groups were estimated before comparison between groups/treatments was carried out and in cases where the assumptions were not met, Greenhouse-Geisser corrections were used. Mean ± SEM values, samples sizes, p values and statistical methods are defined in respective figure legends. No statistical methods were used to pre-determine sample sizes but our sample sizes are similar to those reported in previous publications (e.g., ref 10,19-21). Complete statistics data are reported in "Statistics data reporting by Figure".

References for Methods:

49. Meng, Y. *et al.* Abnormal spine morphology and enhanced LTP in LIMK-1 knockout mice. *Neuron* **35**, 121-133 (2002).
50. Zhou, Z. *et al*. GluA2 (GluR2) regulates metabotropic glutamate receptor-dependent long-term depression through N-cadherin-dependent and cofilin-mediated actin reorganization. *J. Neurosci.* **31**, 819-833 (2011).

Data Availability:

All supplementary information is available in the online version of the paper. All other source data are available from the corresponding author (Zhengping Jia) upon reasonable request.

Fig. 1

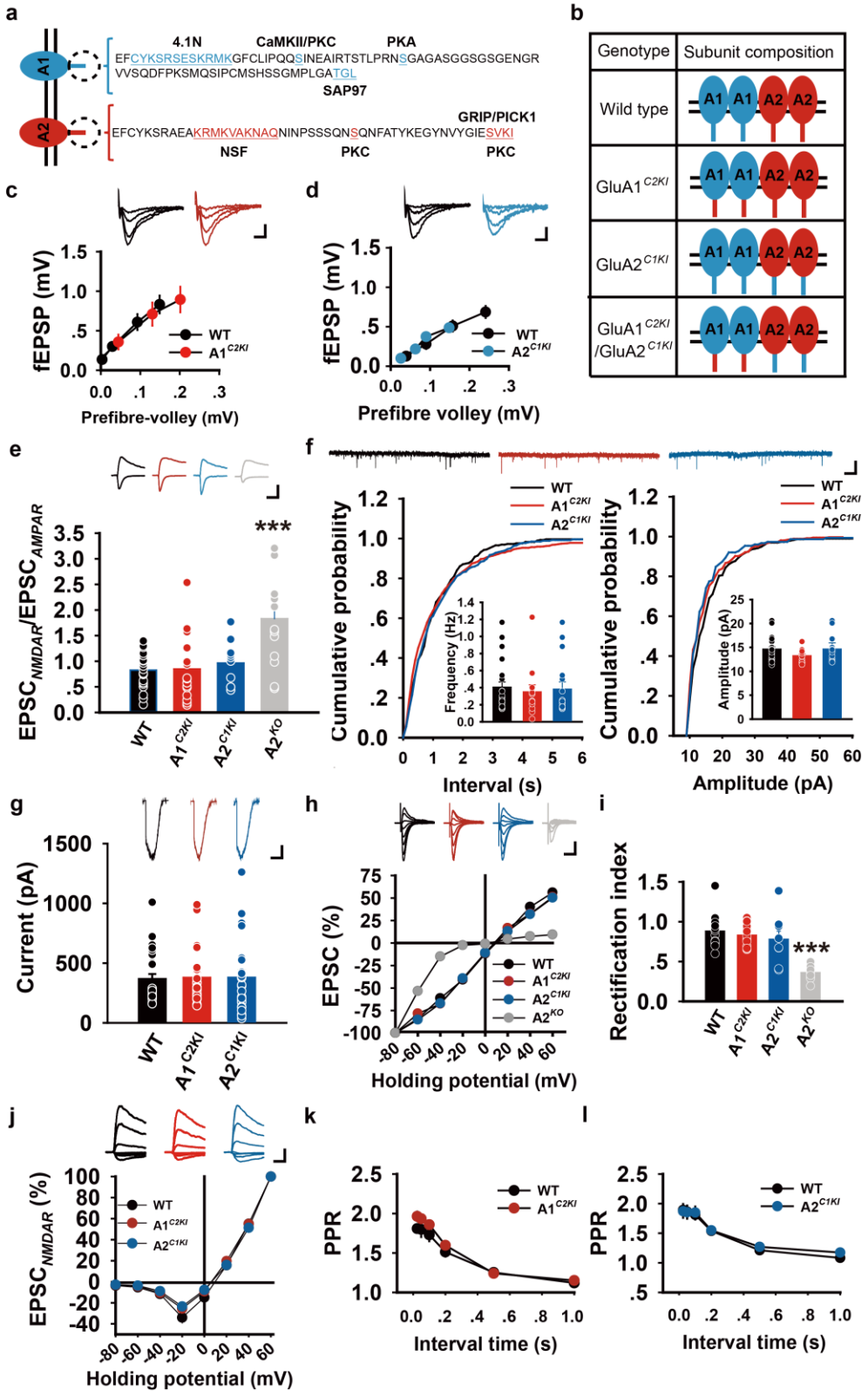
a
4.1N
CaMKII/PKC
PKA
EFCYKSRSESKRMKGFCLIPQQSINEAIRTSTLPRNSGAGASGGSGSGENGR
VVSQDFPKSMQSIPCMSHSSGMPLGATGL
SAP97
GRIP/PICK1
EFCYKSRAEAKRMKVAKNAQNINPSSSQNSQNFATYKEGYNVYGIESVKI
NSF
PKC
PKC
b
Genotype
Subunit composition
Wild type
GluA1 C2KI
GluA2 C1KI
GluA1 C2KI /GluA2 C1KI
c
fEPSP (mV)
Prefibre-volley (mV)
WT
A1 C2KI
d
fEPSP (mV)
Prefibre volley (mV)
WT
A2 C1KI
e
EPSC NMDAR/EPSC AMPAR
***
WT
A1 C2KI
A2 C1KI
A2 KO
f
Cumulative probability
Interval (s)
Frequency (Hz)
Amplitude (pA)
WT
A1 C2KI
A2 C1KI
g
Current (pA)
WT
A1 C2KI
A2 C1KI
h
EPSC (%)
Holding potential (mV)
WT
A1 C2KI
A2 C1KI
A2 KO
i
Rectification index
***
WT
A1 C2KI
A2 C1KI
A2 KO
j
EPSC NMDAR (%)
Holding potential (mV)
WT
A1 C2KI
A2 C1KI
k
PPR
Interval time (s)
WT
A1 C2KI
l
PPR
Interval time (s)
WT
A2 C1KI

Fig. 2

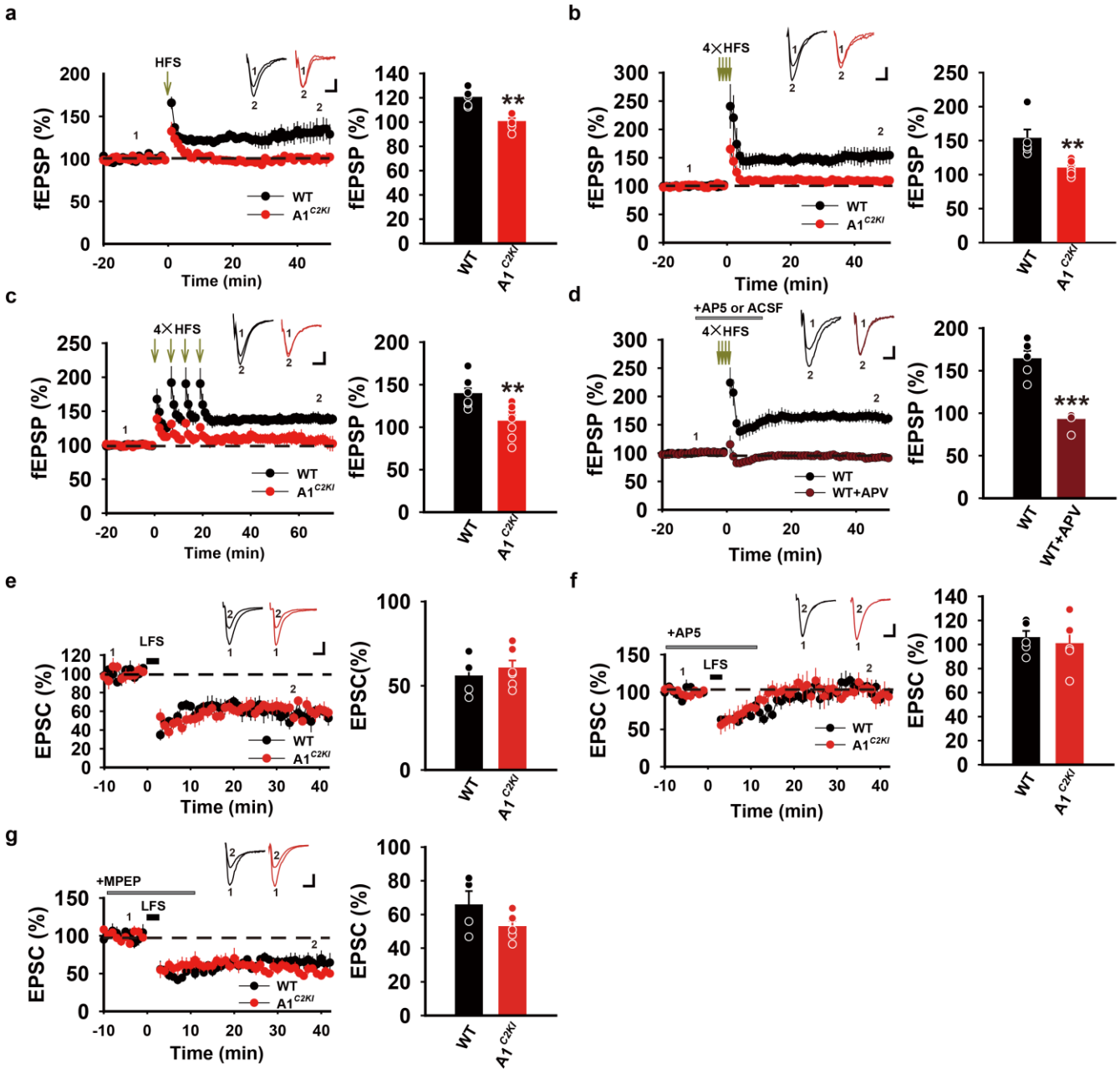
a
HFS
fEPSP (%)
Time (min)
WT
A1 C2KI
**
b
4×HFS
c
4×HFS
d
+AP5 or ACSF
4×HFS
WT+APV
***
e
LFS
EPSC (%)
f
+AP5
LFS
g
+MPEP
LFS

Fig. 3

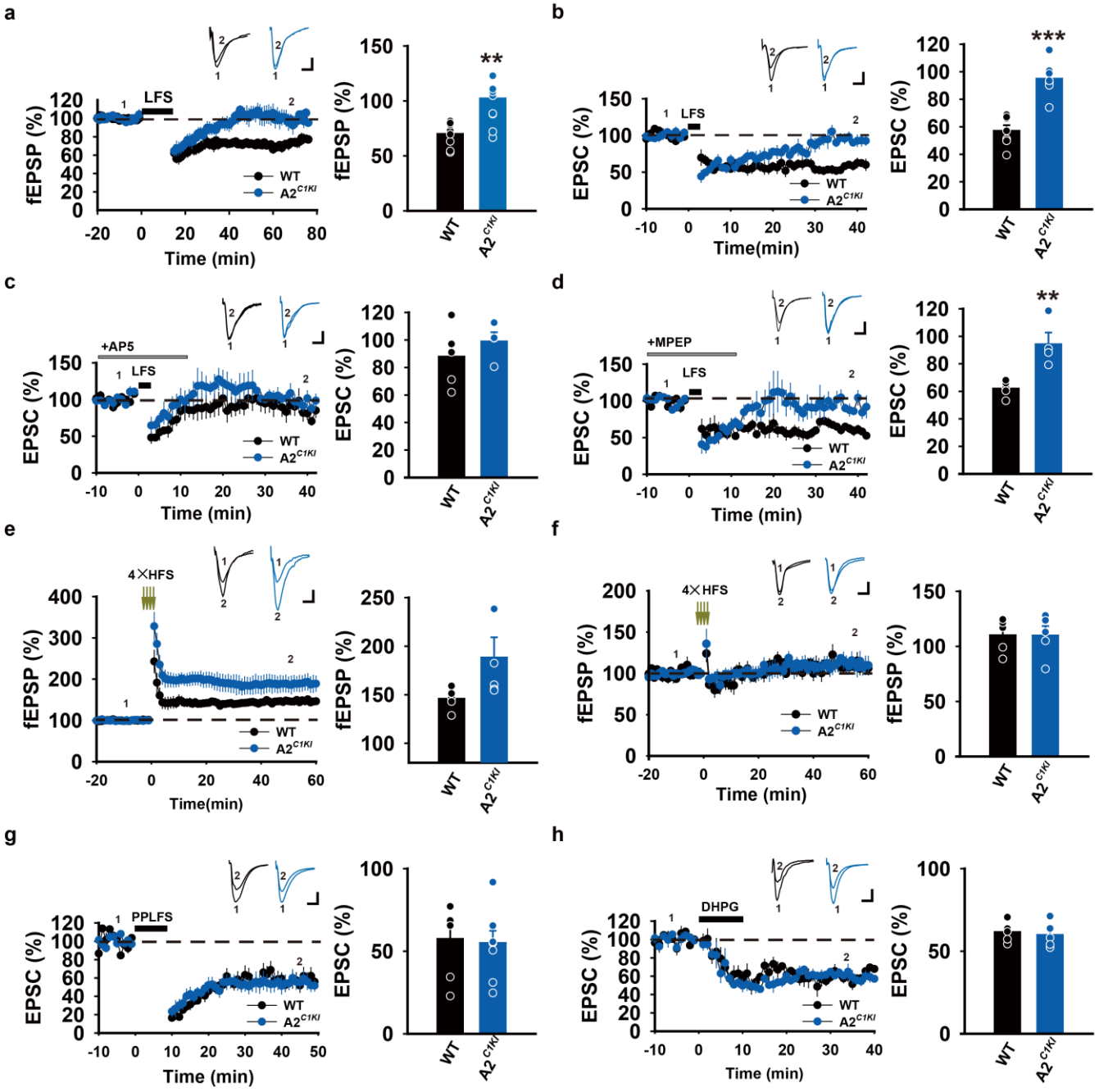
a
fEPSP (%)
LFS
WT
A2C1KI
Time (min)
fEPSP (%)
**
WT
A2C1KI
b
EPSC (%)
LFS
WT
A2C1KI
Time(min)
EPSC (%)
***
WT
A2C1KI
c
+AP5
LFS
EPSC (%)
WT
A2C1KI
Time (min)
EPSC (%)
WT
A2C1KI
d
+MPEP
LFS
EPSC (%)
WT
A2C1KI
Time (min)
EPSC (%)
**
WT
A2C1KI
e
4×HFS
fEPSP (%)
WT
A2C1KI
Time(min)
fEPSP (%)
WT
A2C1KI
f
4×HFS
fEPSP (%)
WT
A2C1KI
Time (min)
fEPSP (%)
WT
A2C1KI
g
PPLFS
EPSC (%)
WT
A2C1KI
Time (min)
EPSC (%)
WT
A2C1KI
h
DHPG
EPSC (%)
WT
A2C1KI
Time (min)
EPSC (%)
WT
A2C1KI

Fig. 4

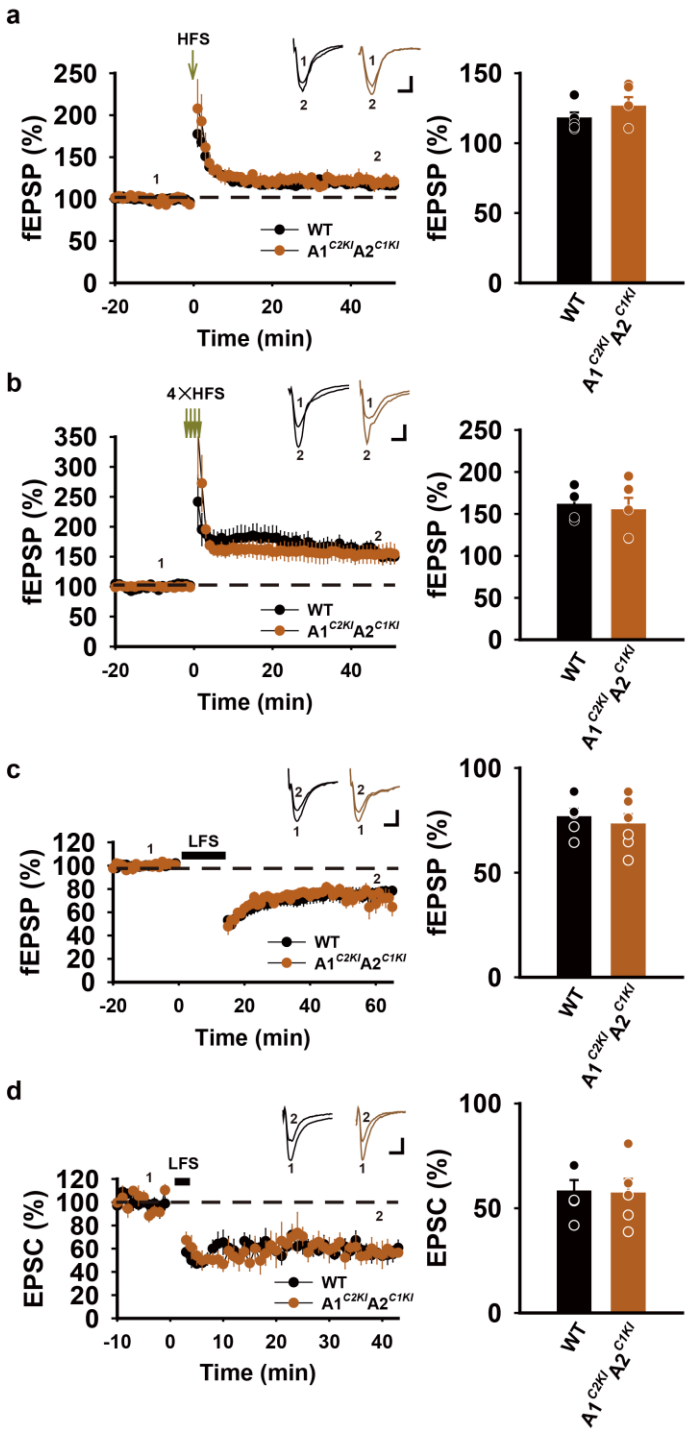

Fig. 5

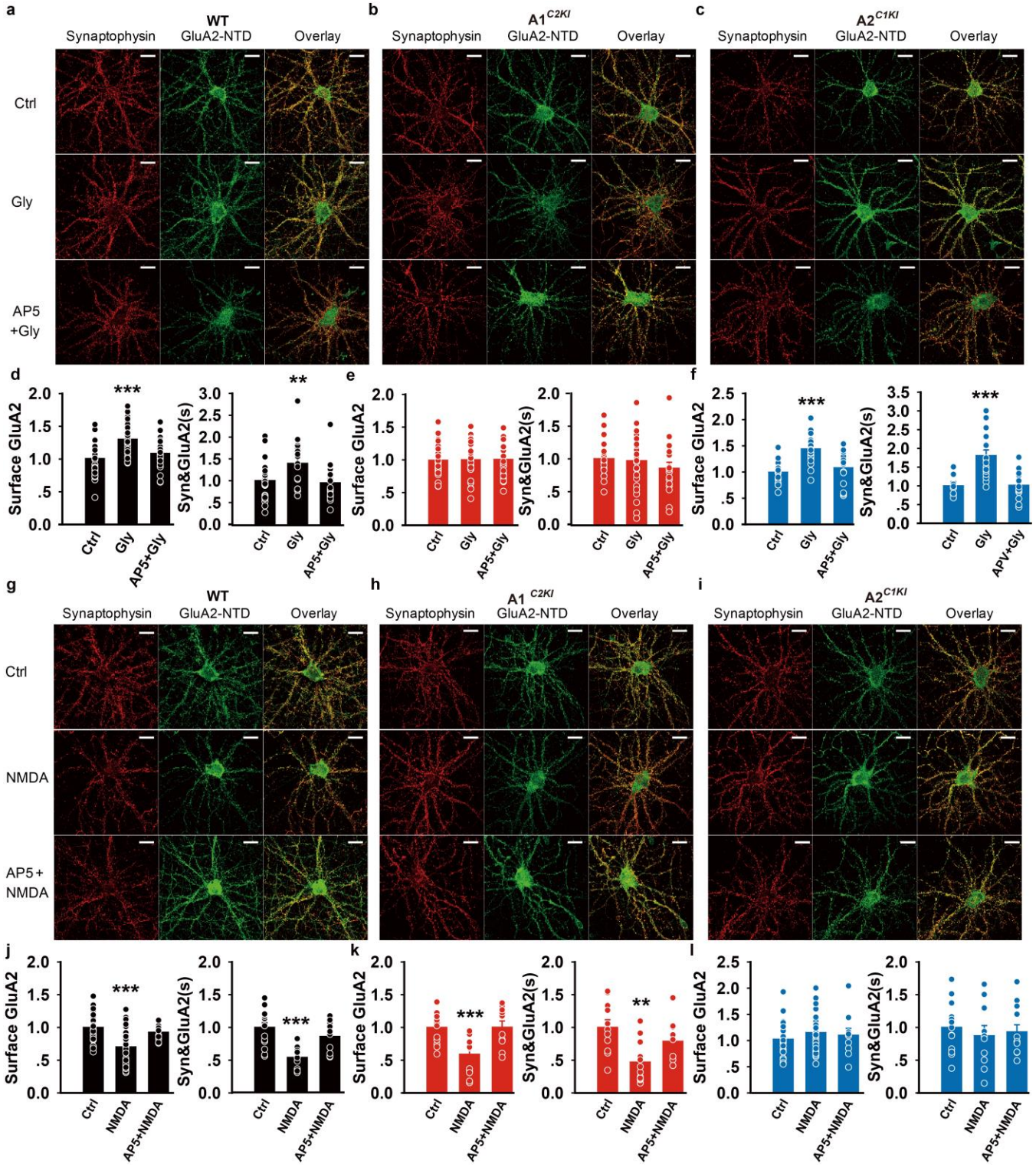
a
WT
Synaptophysin
GluA2-NTD
Overlay
Ctrl
Gly
AP5 +Gly
b
A1C2KI
c
A2C1KI
d
Surface GluA2
Syn&GluA2(s)
***
**
Ctrl
Gly
AP5+Gly
e
f
APV+Gly
g
NMDA
AP5+ NMDA
h
i
j
k
l
AP5+NMDA

Fig. 6

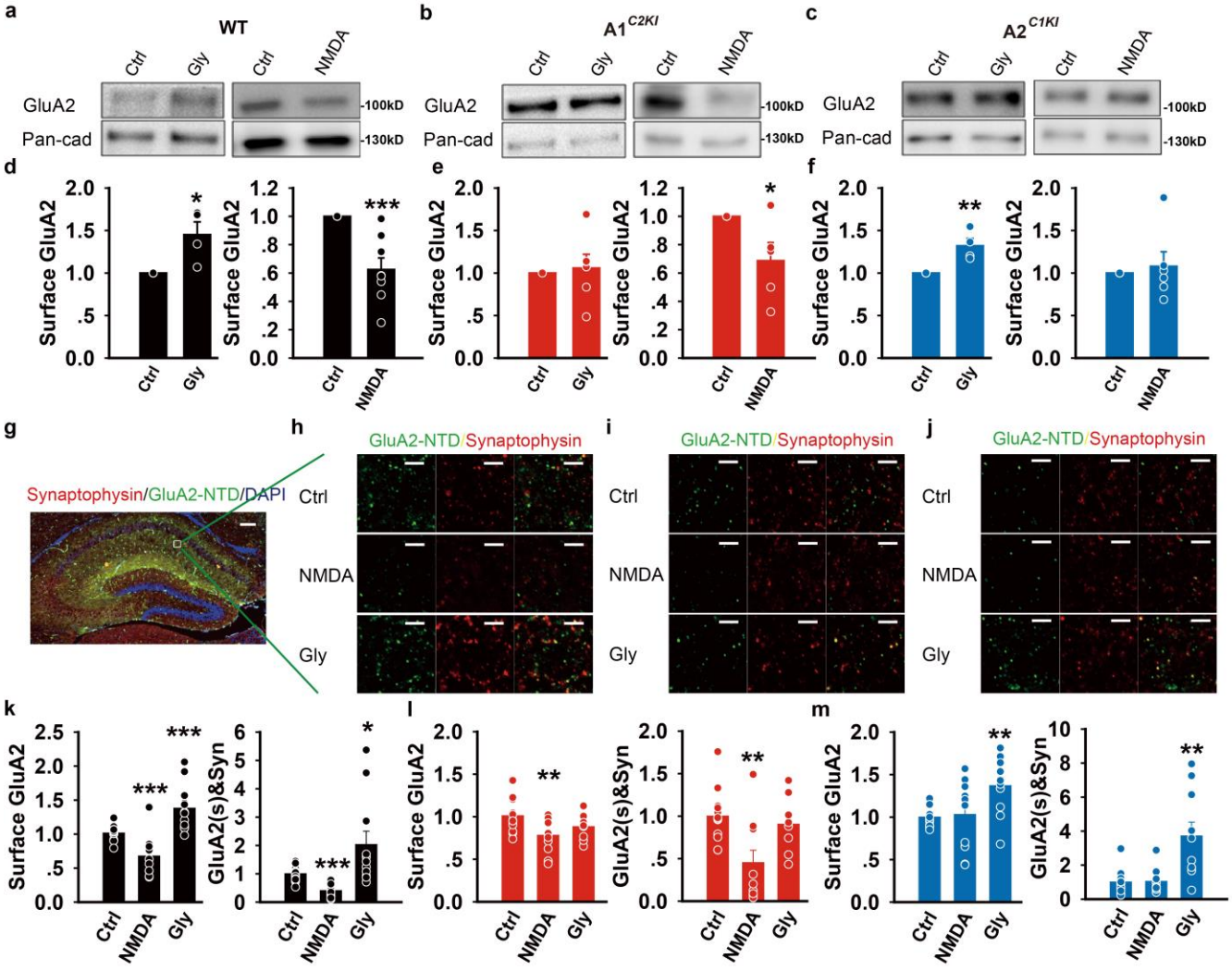
a
WT
Ctrl
Gly
Ctrl
NMDA
GluA2
Pan-cad
100kD
130kD
b
A1C2KI
c
A2C1KI
d
Surface GluA2
e
f
g
Synaptophysin/GluA2-NTD/DAPI
h
GluA2-NTD/Synaptophysin
i
j
Ctrl
NMDA
Gly
k
GluA2(s)&Syn
l
m

Fig. 7

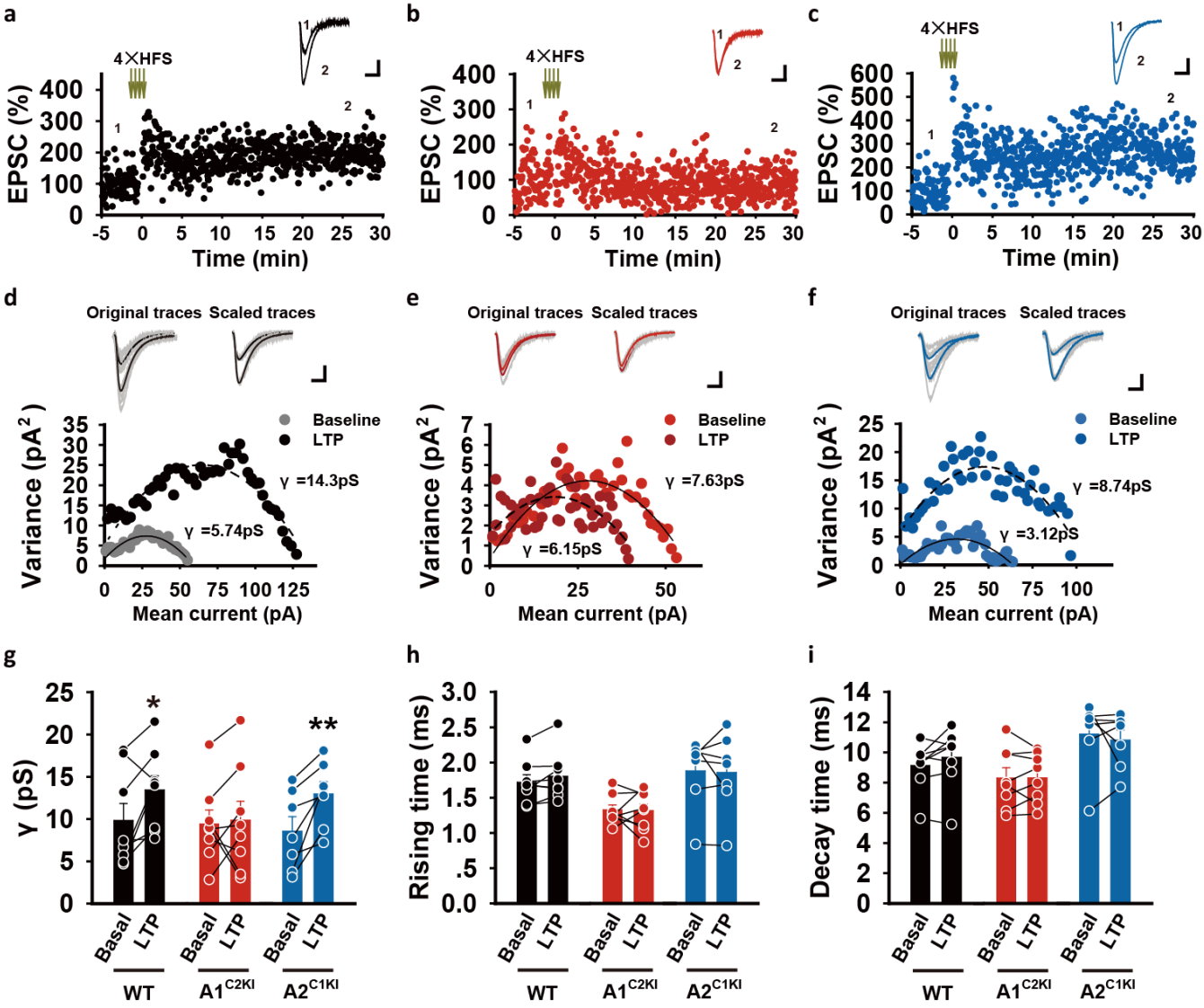
a
b
c
4×HFS
EPSC (%)
Time (min)
d
e
f
Original traces
Scaled traces
Baseline
LTP
Variance (pA²)
Mean current (pA)
γ =14.3pS
γ =5.74pS
γ =7.63pS
γ =6.15pS
γ =8.74pS
γ =3.12pS
g
h
i
γ (pS)
Rising time (ms)
Decay time (ms)
Basal
LTP
WT
A1C2KI
A2C1KI

Fig. 8

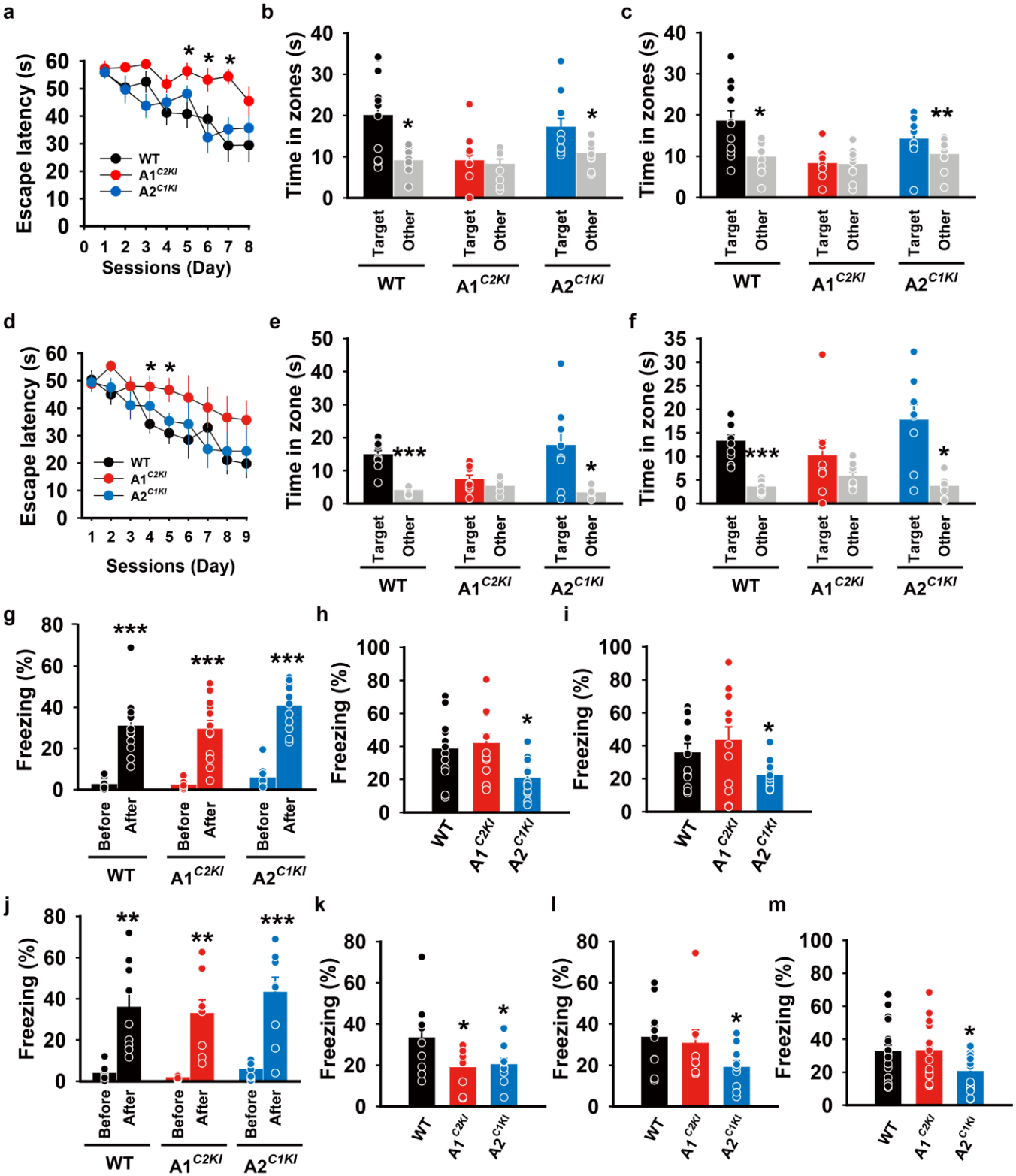
a
Escape latency (s)
Sessions (Day)
WT
A1C2KI
A2C1KI
b
Time in zones (s)
c
Time in zones (s)
Target
Other
WT
A1C2KI
A2C1KI
d
Escape latency (s)
Sessions (Day)
e
Time in zone (s)
f
Time in zone (s)
g
Freezing (%)
Before
After
h
Freezing (%)
i
Freezing (%)
j
Freezing (%)
k
Freezing (%)
l
Freezing (%)
m
Freezing (%)